Tampere University

Aaron Rogers

WAVELENGTH TUNABLE MECSELS

Master's Thesis
Faculty of Natural Sciences
Examiner/s: Mircea Guinea, Philipp Tatar-Mathes
May 2023

ABSTRACT

Aaron Rogers: Wavelength Tunable MECSELs
Master's Thesis
Tampere University
May 2023

Membrane external-cavity surface-emitting lasers (MECSELs) represent a relatively new category of semiconductor laser that have potential to be attractive tunable light sources for various applications. Potential advantages over similar lasers include improved active region heat extraction, access to novel wavelength regimes, and wider tuning ranges. Semiconductor membranes with varying quantum well architectures were investigated in this thesis. Additionally, varying cavity configurations and intracavity elements were investigated with the goal of satisfying application-specific properties required for implementation.

Keywords: MECSEL, laser, semiconductor, tunable-laser

CONTENTS

LIST OF FIGURES

LIST OF ACRONYMS

DBR	Distributed Bragg reflector
MBE	Molecular-beam epitaxy
MECSEL	Membrane external-cavity surface-emitting laser
MOVPE	Metal organic vapor-phase deposition
OCT	Optical coherence tomography
PL	Photoluminescence
QW	Quantum well
RPG	Resonant periodic gain
RTA	Rapid thermal annealing
SiC	Silicon carbide
Ti:Sa	Titanium-sapphire
VCSEL	Vertical-cavity surface-emitting laser
VECSEL	Vertical external-cavity surface-emitting laser

1 INTRODUCTION

Since their invention by Maiman in 1960, lasers have found use in a multitude of applications, including diverse topics such as lidar, gas sensing, metal etching, and telecommunications, among many others. There are also many types of lasers, where examples include: solid state, gas, dye, free-electron, semiconductor, etc... This thesis however explores the use of a type of semiconductor laser, the membrane external-cavity surface-emitting laser (MECSEL), and its ability to be used as a tunable light source. Semiconductor lasers are diverse, with the most common form being laser diodes which are essential elements of CD players, printers, barcode scanners, and many other common applications. The type of semiconductor described in this thesis, the MECSEL, has a few key differences from a conventional laser diode which will be described. While many different modalities of lasers can be used to achieve a tunable light source, MECSELs offer a unique profile of parameters that could prove advantageous.

Semiconductor lasers are quite cheap and easy to tailor, which makes them attractive sources for a wide range of applications. Within the field of semiconductor lasers, surface emitters have the potential for both high beam quality and high power. MECSELs offer additional considerations as well, and to understand these fully it is useful to first look at the development and creation of this subset of laser. Other tunable lasers and the way in which MECSELs compare will be explored in the **Application Context and Motivation** chapter. A complete picture of MECSELs and how they can be applied in a potential application requires a theoretical background in semiconductor and laser physics. This will be encapsulated in the **MECSEL Background** chapter. Moving forwards, the design of the various experiments that were undertaken as part of this thesis, alongside the measurements that took place will be explored in the **Experimental Setups and Measurements** chapter. The contents of the thesis will be reviewed and discussed further in the **Summary and Outlook** chapter. Additionally, the potential for MECSELs to be implemented as a commercial device will be explored throughout the contents of this thesis.

2 APPLICATION CONTEXT AND MOTIVATION

Wavelength tunable lasers are used in a wide range of applications, covering fields such as telecommunications, material processing, medicine, spectroscopy, and many more. Each of these applications brings its own specifications in laser properties. Example properties include power, beam diameter, beam quality, linewidth, cost, size, ease of use, etc. This gives rise to a wide variety of tunable lasers and laser systems on the market and in research labs across the world.

While the very first laser was created by Maiman in 1960, the first practical tunable laser was introduced in 1966 by Sorokin and Lankin [1] and Schäfer et al. [2]. This first tunable laser was a dye laser, which uses a liquid organic molecule in a solvent. Being the first tunable laser, dye lasers naturally created "... a large body of scientific literature" [3]. Inherent issues with dye lasers lead to a new tunable laser technology, the titanium-sapphire laser, becoming more popular. The titanium-sapphire (Ti:Sa) laser was invented in 1968 by P.F. Moulton [4] and quickly became the laboratory standard for both tunable and ultrafast lasers in the red to near-infrared regime. This is still true, and sales of Ti:Sa lasers are expected to continue to grow throughout the 2020's. However, there are drawbacks to Ti:Sas, such as the expensive and sensitive pumping schemes required, and complex large cavity configurations. Conventional semiconductor lasers such as diodes are much cheaper and have the potential for tuning, but present other issues such as the tuning range and beam quality. Based on the criteria of high-power, broad tunability, excellent beam quality, and lower price, the MECSEL is a potential candidate, and that potential is explored throughout this thesis.

The MECSEL is a variation on the better-known vertical external-cavity surface-emitting laser (VECSEL) which was created in 1997 by Kuznetsov [5] to "overcome a key problem with conventional semiconductor lasers: how to generate watt-level and higher optical powers with fundamental transverse mode circular optical beam quality" [6]. The MECSEL contrasts with the VECSEL in that instead of having a mirror as part of the semiconductor structure, the MECSEL is a thin membrane that only uses external mirrors. This membrane design offers advantages, such as superior heat extraction, double-side pumping, and more. The MECSEL is an extremely new approach that was demonstrated in 2015-2016 [7],[8]. There are various benefits and challenges of the MECSEL architecture, and a benefit inherently related to wavelength tunability is the lack of a DBR, a semiconductor mirror that has broadband limitations. The creation of the MECSEL and its applicability as a tunable source will be covered in more detail in the following chapter.

3 MECSEL THEORETICAL BACKGROUND

3.1 MECSEL Background and Theory

The MECSEL is a niche, modern semiconductor device/concept. Understanding what sets this device apart is best viewed from a developmental lens, beginning with work done by Einstein over a hundred years ago and leaving us with the various groups working on the MECSEL concept today. Along with this historical background, the corresponding physics will be explained.

The term **LASER** has been used ubiquitously such that the acronym, Light Amplification by Stimulated Emission of Radiation, is not so well known. The acronym itself points us to the underlying history and work necessary for the creation of the laser, a theory of stimulated emission. Einstein published a paper in 1916 titled *On the Quantum Theory of Radiation* that introduced the concept of stimulated emission and the treatment of light as a quantum phenomenon. Since lasers are based on stimulated emission, a quantum process, they are fundamentally quantum devices. While lasers can be incredibly complex, only three things are essentially needed: an energy source (pump), an optical resonator (a simple cavity could consist of two mirrors facing each other), and gain (a way for pump energy to be converted through stimulated emission into laser energy).

Before the creation of the laser, a similar scheme was investigated that took advantage of a different part of the electromagnetic spectrum. The maser, which stands for microwave amplification by stimulated emission of radiation, was invented by Townes in 1955 [9]. Not long after the maser was invented, the first laser, a ruby rod optically pumped with a flash lamp, was created by Maiman in 1960. [10]. A laser constituting a crystal like the aforementioned device is an example of a solid-state laser. Other laser modalities were investigated and created soon after, the first being a helium-neon gas laser, where the photon energy is determined by an atomic transition, in 1961 by Jaivan et al [11]. A semiconductor-based laser, the class of laser investigated in this thesis, was first demonstrated by Hall et al in 1962 [12]. This laser was a gallium arsenide (GaAs) p-n junction based device. A p-n junction refers to how a semiconductor can be positively, "p", and negatively, "n", doped. Specifically, negative doping would mean an abundance of electrons, while positive would be a lack of electrons where that "lack of electron" is referred to as a hole, so positive doping would give an abundance of holes. P-n junctions are widespread across semiconductor devices and can be used as a way to electrically pump a laser. An electron can recombine with a hole, and the energy difference between the

two can be released as a photon [13]. This mechanism is how a p-n junction can be used to achieve lasing but will not be explored further as p-n junctions are a strategy for electric pumping, and are not incorporated in MESECLs as they are optically pumped.

The first semiconductor lasers were radically different than the ones that exist today. They required extremely cold temperatures and pulsed operation to function. Improvements have been made sequentially, leading to the advanced diodes and other semiconductor lasers such as MECSELs that exist today. Nikolay Baslov introduced new concepts to semiconductor lasers in a 1966 paper [14]. Efficient and convenient heat extraction with a "cold finger" (now regularly called a heat sink or heat spreader), the use of external mirrors, and using a thin slice of semiconductor material as the active region, which is described as a "radiating mirror" were advancements he discussed. These advancements are fundamental to the MECSEL principle.

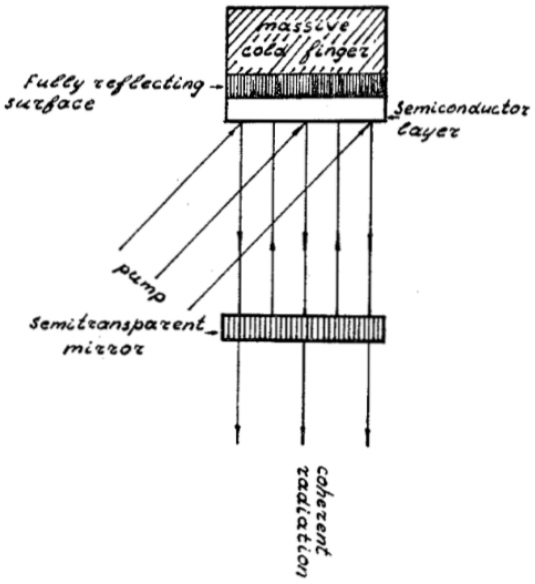

Figure 3.1. *Semiconductor laser with radiating mirrors, pump, semitransparent mirror, and cold finger. Coherent radiation (the laser beam) is generated by the semiconductor layer and passes through the semitransparent mirror. (Fig. from [15]).*

This basic schematic is the foundation which with a few tweaks can be applied to many external cavity semiconductor lasers.

Moving forward, continuous wave semicondcutor devices were demonstrated with the aid of a new heterojunction design theorized by Kroemer in 1963 [16]. Continuous wave refers to a laser emitting continually in contrast to pulsed modalities, and heterojunction refers to an interface between two different types of (usually) lattice matched semiconductor materials, which would also have different bandgap energies. To get into what lattice matching and bandgap energy means, let's take a step back to the physics.

3.2 The Semiconductor Lattice

Semiconductors are crystals, and a crystal has the properties that its atoms are a regular and repeating distance apart with a specific geometry. This is in contrast to amorphous materials like rubber or glass, or polycrystalline materials like most rocks.

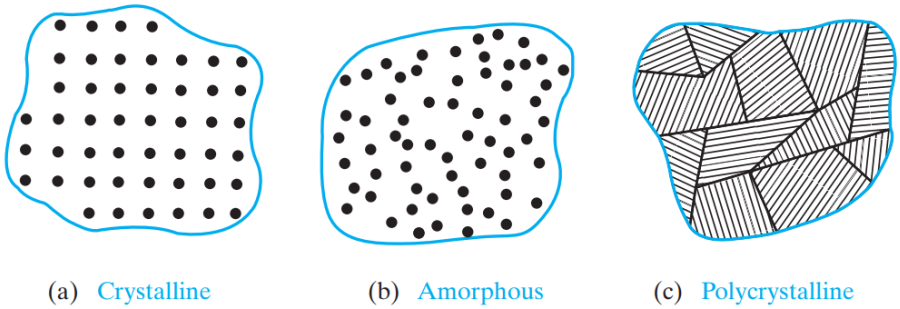

Figure 3.2. *"Three types of solids, classified according to atomic arrangement: (a) crystalline and (b) amorphous materials are illustrated by microscopic views of the atoms, whereas (c) polycrystalline structure is illustrated by a more macroscopic view of adjacent single-crystalline regions, such as (a)" (Fig. from [17])*

Crystals can have different structures, such as the simple case where an atom resides at each corner of a cube, known as simple cubic. For semiconductor structures, a common crystal structure is called face-centered cubic:

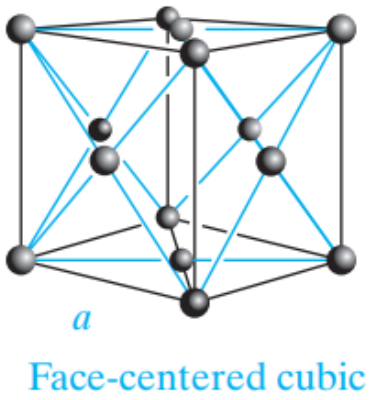

Figure 3.3. *Illustration of a face-centered cubic unit cell (Fig. from [17])*

where a is the lattice constant. This view is of the unit cell, which is the smallest repeating cube, such that the entire crystal consists of this cube repeated periodically. The lattice constant of a material is often given in ångströms, an example of which is that silicon has a lattice constant of approximately 5.43 Å. When growing a semiconductor on top of another semiconductor, an important consideration is that the lattice constants of the two semiconductors are nearly equal. If they are not equal, strain will be introduced which will cause "misfit dislocations" [17] and make the structure not suitable for most devices. The situation is further complicated in the way that a thin layer can manage a sizable amount

of strain, where the growth is called pseudomorphic growth, but if a critical thickness is reached, these mismatches will occur. The lattice value for a semicondcutor consisting of ternary (comprised of three) semiconductor components like InGaAs can be calculated using Vegard's law.

$$a_{A_{1-x}B_xC} = (1-x)a_{AC} + xa_{BC} \tag{3.1}$$

Here, $a_{A_{1-x}B_xC}$ is the lattice constant for the ternary compound, a_{AC} and a_{BC} are the lattice constants of the binary alloys InAs and GaAs respectively, and x is the molar fraction of compound B.

This equation can be extended for a quarternary compound like AlGaInP as well.In addition to the lattice constant, the bandgap is a value that needs to be understood analytically. The bandgap energy for a semiconductor is more complicated to calculate than the lattice constant, and the relationship between the two can be seen below for the examples of InGaAsP and AlGaAsSb material systems.

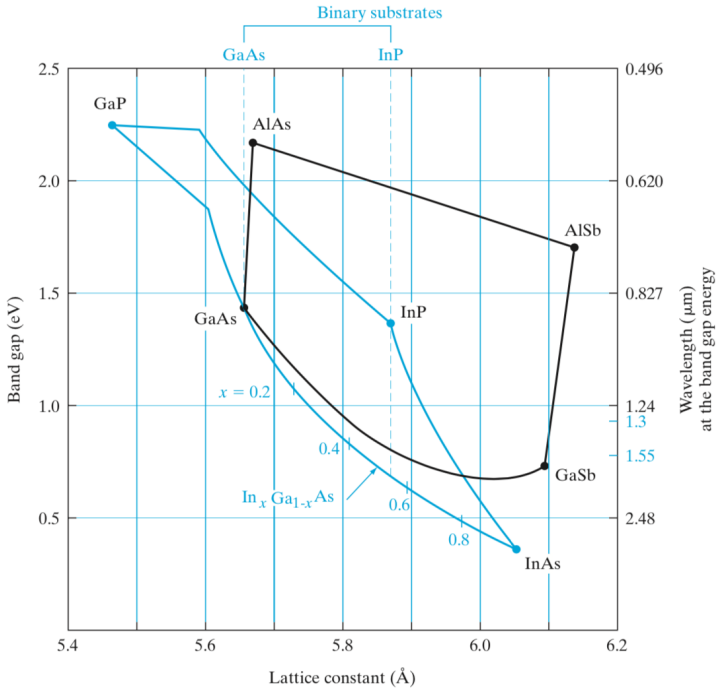

Figure 3.4. *Relationship between band gap energy and lattice constant for alloys in the InGaAsP and AlGaAsSb material systems. (Fig. from [17]).*

While lattice constant is linear with variation in alloy percentage, the bandgap energy is often calculated with the use of a quadratic bowing parameter:

$$E_{A_xB_{(1-x)}C} = E_{AC}x + E_{BC}(1-x) + x(1-x)b \tag{3.2}$$

which has the same variable designations as Vegard's Law, but with the addition of the

bowing parameter b. Understanding the lattice constant and bandgap allows for the engineering of precise heterostructures.

An electron hole pair is generated when an electron is excited from the valence band to the conduction band. In a semiconductor, this looks like:

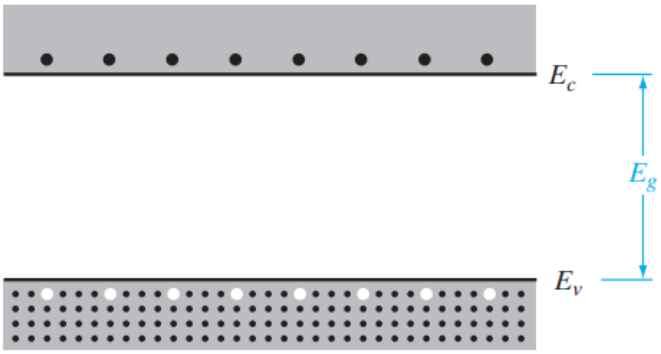

Figure 3.5. *Direct transition with accompanying photon emission (Fig.from [17]).*

where E_v is the valence band energy, E_c is the conduction band energy, and E_g is the difference between the two called the bandgap. An electron in the valence band can be excited to the conduction band and leave behind a hole by absorbing energy, be it thermal, electric, or a photon. When an electron hole pair decays through direct recombination, this energy can result in the generation of a photon:

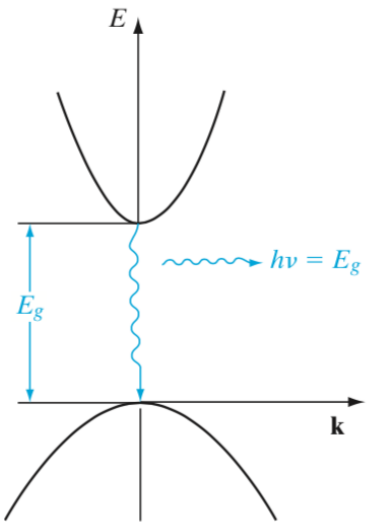

Figure 3.6. *Direct transition with accompanying photon emission (Fig.from [17]).*

where h is Planck's constant, ν is the frequency of the emitted wave, E is energy, and the **k** refers to k-space, also called momentum space. The relationship shows that the energy of the photon is equal to the bandgap of the semiconductor. Additionally, direct

recombination means that there is not a change in momentum, or **k**. From an application standpoint, lasers and LEDs require direct recombination, which is why silicon and other materials with indirect bandgaps are not used for these types of optoelectronic devices. Understanding K-space can be quite confusing and is not directly required to understand the MECSEL concept, so it will be explained more but briefly. If one looks at the k-space diagrams for Si and GaAs:

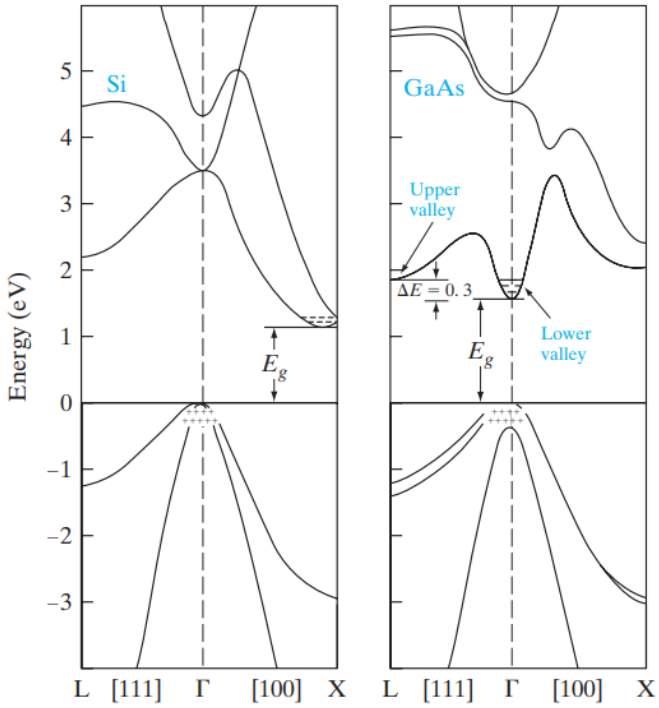

Figure 3.7. *"Conduction and valence bands in Si and GaAs along [111] and [100]" (Fig.from [17]).*

where Γ is the **k**=0 point, and χ and L along with Γ are points of symmetry in the Brillouin zone. The Brillouin zone is the primitive cell for k-space. From this diagram, where the positive valued curves describe electrons and the negative value curves describe holes, it can be seen that the lowest electron "valley" is at the same point in k-space (horizontal axis) for GaAs, and not for Si.

Strain was mentioned as something to be avoided in the previous text on lattice matching, however there can be certain benefits. By applying compressive or tensile strain, the light hole (LH) and heavy hole (HH) can be moved up and down in energy. The naming of heavy and light hole band comes from the fact that the effective mass of a hole is related to the its curvature. Compressive strain is usually used as it leads to a situation where the holes are in the heavy hole band, which has a faster transition rate than the light hole band [18]. Additionally, heavy hole band lasing prefers TE vs. TM polarization.

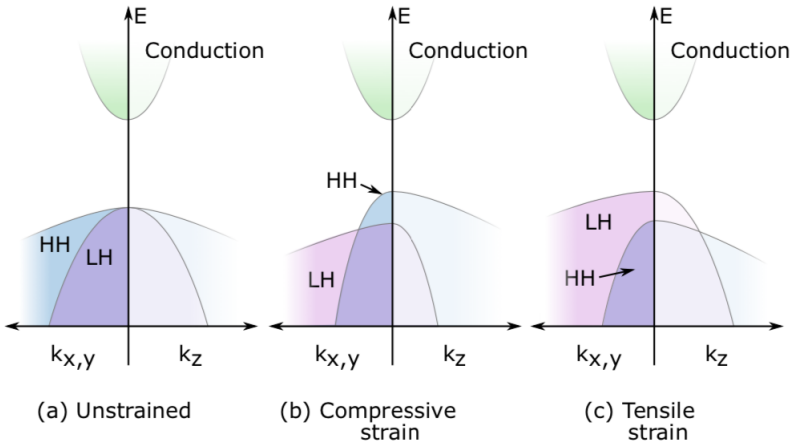

Figure 3.8. *Effect of strain on the heavy hole and light hole bands. (Fig.from [7]).*

Fig. 3.4

Now that the physics has been covered, the developmental background of the MECSEL can be further explored.

3.3 Vertical Cavity Lasers

The first laser created by Maiman and the semiconductor lasers that were developed shortly after were all edge-emitting lasers, in contrast to the other possibility, vertical emitting. An easy way to picture the difference is to think of the gain chip as a rectangular piece of cardboard. An edge emitter would have propagation inside the paper parallel to the surface, while a vertical emitter would consist of light only passing through the small thickness of the paper, and emitted perpendicular to the surface of the paper. The following schematics show this difference, along with some other key elements of the lasers. The first image is a standard edge-emitting laser diode, and the second image is of a vertical cavity surface-emitting laser (VCSEL).

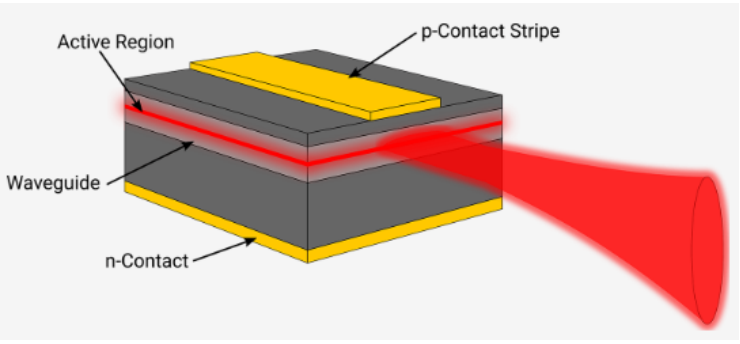

Figure 3.9. *An edge emitter, the original laser design. (Fig. from [19]).*

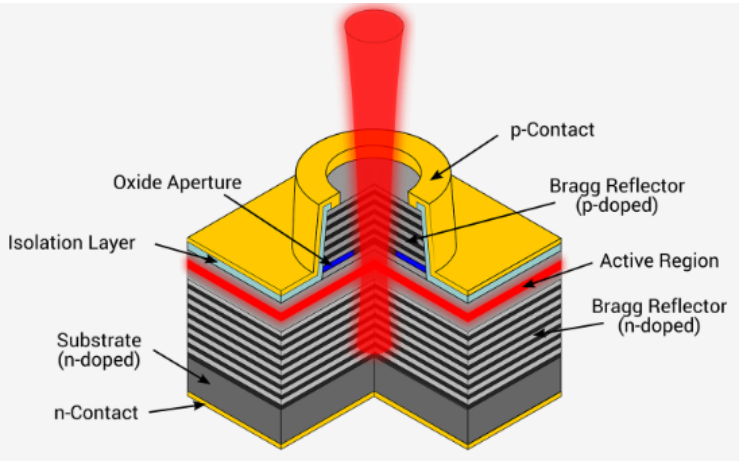

Figure 3.10. *A VCSEL, a type of vertical emitter that offers compactness and beam quality (Fig. from [19]).*

VCSELs started out only operating at liquid nitrogen temperatures [20] and the authors had predictions for how room temperature operation could be achieved: "To realize easy room temperature oscillation, it would be necessary to adopt some new structures such as multilayer dielectric mirrors, quantum well structure, and so on [20]". The prediction the authors made about dielectric mirrors can be seen in Fig. 3.10, as a "Bragg Reflector", which will be called a distributed Bragg reflector (DBR) in this thesis, is incorporated into the device. A DBR is a type of mirror that relies on two different alternating optical materials stacked periodically. The thickness of each layer conventionally corresponds to one-quarter of the wavelength of light that is to be reflected. This thickness needs to take the refractive index of each material into account such that:

$$d = \frac{\lambda}{4n} \tag{3.3}$$

where d is the layer thickness, lambda is the wavelength of light to be reflected (in vacuum), and n is the refractive index of the material. The DBR is superior to a cleaved facet in a few ways, one being the potential for monolithic growth, and another being higher reflectivity R. Monolithic growth refers to all of the various semiconductor layers being grown on top of each other as part of a single crystal. How semiconductors can be grown will be touched on later. The reflectivity (a specific instance of reflectance) can be approximated as:

$$R = \left[\frac{n_o(n_2)^{2N} - n_s(n_1)^{2N}}{n_o(n_2)^{2N} + n_s(n_1)^{2N}}\right]^2 \tag{3.4}$$

where N is the number of pairs, n_o is refractive index of the originating material, n_1 is the refractive index of one of the alternating layers, n_2 is the refractive index of the other, and n_s is the refractive of the backside of the DBR which could the substrate. To get maximum reflectance, semiconductors with highly different refractive indices should be

used, alongside with as many layers.

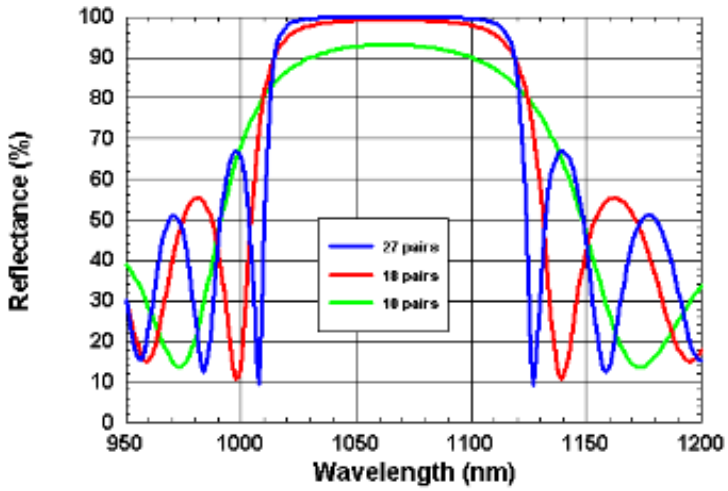

Figure 3.11. *Model of DBR reflectance (related to reflectivity) (Fig. from [21]).*

This gives rise to tailored DBRs where the reflectivity of a DBR mirror can be chosen with these other parameters in mind. A common example of this would be to create a "front" and "back" DBR, where the back mirror is highly reflective with a reflectivity of >99 %, and the front mirror could be around 95 % [20].

Another consideration when looking at vertical cavity design is the significantly shorter gain region compared to edge emitting lasers. In an electrically pumped scheme, this leads to a pumping situation where, "threshold current density is much higher than the conventional laser diode" [22]. This is a direct result of less propagation through gain comparatively which is compensated for with higher current density. A further challenge is observed when trying to get more a larger beam, which would be useful for higher output power, from a VCSEL. The design for electric pumping of a VCSEL as seen in [**fig:VCSEL**] has the key limitation that expanding the size of the circular contact leads to inhomogenous pumping and failure of the laser. The challenge of larger pumped regions leads directly to the creation of the vertical external-cavity surface-emitting laser (VECSEL), also called a semiconductor disk laser.

3.4 VECSELs

The task of building a VECSEL was undertaken in 1995 by Micracor (spearheaded by Aram Mooradian) [23], although the term optically pumped semiconductor laser was used at the time. VECSELs (and modern VCSELs) take advantage of a double heterojunction called a quantum well. Quantum wells describe a thin layer of material that is placed between two other materials, and if this thickness is near the DeBroglie wavelength, quantum effects will be relevant. Quantum wells offer multiple benefits, including increased customizability since the width of the well has an effect on the bandgap, and allow for efficient recombination of electron hole pairs. While quantum wells are very effective sites for

recombination, they are quite inefficient at absorbing pump light, so the common strategy is to pump the barriers, and allow the electron hole pairs to migrate to the quantum wells. There is a strategy called in-well pumping where the wells are pumped, but with this low absorption, complex pumping schemes are required. Additionally, a specific wavelength is required for in-well pumping whereas barrier pumping can be done by a huge range of wavelengths. The benefit of in-well pumping is that the quantum defect, which is the difference in energy between the photons for pumping and the photon energy of the laser beam, is smaller. This energy is lost as heat, and is the minimum amount of heat that will be generated by operation of the device even if there were no other imperfections, which of course there are. The sensitivity, cost, and restrictions imposed by in well pumping are why it is not used in this thesis and not in most VECSELs and MECSELs.

A standing wave is created in a laser cavity, and as energy is the square of amplitude, the spots of high energy are at the peaks and troughs of the wave. To have the most interaction with the quantum wells, the places where stimulated emission can occur, a resonant periodic gain (RPG) structure is created. This structure looks like:

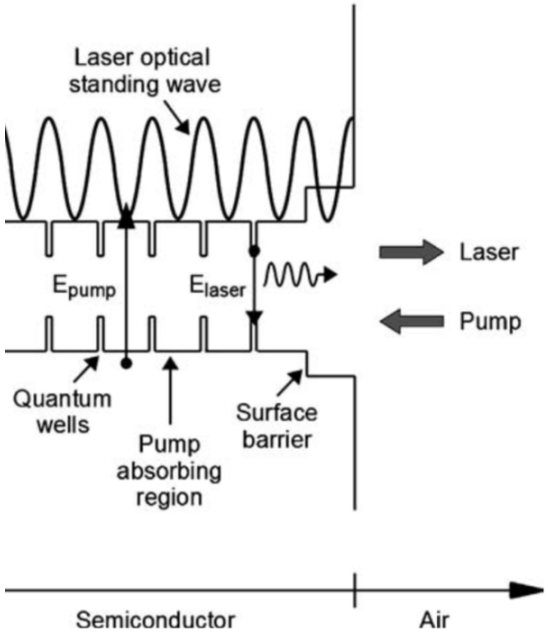

Figure 3.12. *VECSEL/MECSEL operating principles and RPG structure. (Fig.from [6]).*

where E_{pump} and E_{laser} are the energies of the pump and laser photons. This picture is somewhat of a simplification, as quantum wells are generally so small that they are grouped into packets, where a packet of around 3 quantum wells can be in one antinode.

While on the topic of VECSELs, it will be useful to dive into some of the equations that govern VECSEL operation, and of course MECSEL operation as well. The model used here is from Kuznetsov's 1997 paper [5], so the model will be referred to as the Kuznetsov model. This model was described in the author's bachelor's thesis [24], and is restated

here.

3.5 Kuznetsov Model

$$R_1 R_2 T_{\text{loss}} e^{2\Gamma g_{\text{th}} N_{\text{w}} L_{\text{w}}} = 1 \tag{3.5}$$

where R_1 and R_2 are the reflectivities of the mirrors, T_{loss} is the transmission factor (round-trip losses that could be scattering and absorption due to air or dust), and Γ is the longitudinal confinement factor which describes the overlap between the QWs and the standing wave in the active region. Additionally, g_{th} is threshold material gain, N_{w} is the amount of QWs, and L_{w} is the thickness of the QW. Gain g can generally be given by:

$$g = g_0 \ln \frac{N}{N_0} \tag{3.6}$$

where g_0 is the material gain coefficient, N is the carrier density, and N_0 is the transparency carrier density. The material gain coefficient and transparency carrier density are fixed values for a given material, but the carrier density N depends on the properties of the pump source and is given by:

$$N = \frac{\eta_{\text{abs}} P_{\text{pump}}}{E_{\text{ph}} N_{\text{w}} L_{\text{w}} A_{\text{pump}}} \tau(N) \tag{3.7}$$

where η_{abs} is the pump absorption efficiency, P_{pump} is the pump power, E_{ph} is the photon energy, and A_{pump} is the area of the pump spot. Finally, carrier lifetime $\tau(N)$ is a function of the carrier density, given by:

$$\frac{1}{\tau(N)} = A + BN + CN^2 \tag{3.8}$$

where A is the monomolecular recombination coefficient, B is the bimolecular recombination coefficient, and C is the Auger recombination coefficient. Auger recombination becomes more relevant when the target application requires high maximum power, as Auger recombination creates a positive reinforcement loop of heat generation in the active region under high pump conditions. Using the given equations, an equation for threshold carrier density N_{th} and threshold pump power P_{th} can be derived:

$$N_{\text{th}} = N_0 \left(\frac{1}{R_1 R_2 T_{\text{loss}}} \right)^{(2\Gamma g_0 N_{\text{w}} L_{\text{w}})^{-1}} \tag{3.9}$$

$$P_{\text{th}} = \frac{N_{\text{th}} E_{\text{ph}} N_{\text{w}} L_{\text{w}} A_{\text{p}}}{\eta_{\text{abs}} \tau(N)} \tag{3.10}$$

This leads to an expression for the laser's output power P_{laser}, which is given by:

$$P_{\text{laser}} = (P_{\text{pump}} - P_{\text{th}}) \cdot \eta_{\text{diff}} \tag{3.11}$$

where η_{diff}, differential efficiency, is:

$$\eta_{\text{diff}} = \eta_{\text{out}} \cdot \eta_{\text{quant}} \cdot \eta_{\text{abs}} \tag{3.12}$$

While η_{abs} is a value fixed by the given material, η_{out} and η_{quant} are given by:

$$\eta_{\text{out}} = \frac{\ln(R_2)}{\ln(R_2 R_1 T_{\text{loss}})} \tag{3.13}$$

$$\eta_{\text{quant}} = \frac{\lambda_{\text{pump}}}{\lambda_{\text{laser}}} \tag{3.14}$$

where R_2 is the reflectivity of the output mirror. The differential efficiency is one of the critical values of interest in a laser system and will be touched on in the experimental section. Now that a theoretical basis has been set, the path to MECSEL creation can be explored further.

Looking at how VECSELs contrast with VCSELs, VCSELs operate in the 10-100 mW regime while VECSELs have been demonstrated up to 106 W of output power [25]. Additionally, the external cavity in VECSELs allows for the insertion of optical elements like birefringent filters for tuning or nonlinear crystals for frequency doubling. There are certain applications, such as nonlinear frequency doubling and biomedical treatments where both diffraction limited beam quality and high power are required. Furthermore, VECSELs have been used as lasers for generation of short pulses, especially mode-locking, and as tunable sources [26], [27].

However, there are limitations that VECSELs have that arise from the incorporation of a DBR. Semiconductor material is a poor thermal conductor compared to commonly used heat spreader materials like SiC, sapphire, and especially diamond. VECSEL chips were originally bonded to heat spreaders from the very thick substrate, which the DBR and then active region were on top of. This method was improved by two methods, flip-chip and intracavity heat spreader. Flip-chip consists of growing the structure the opposite way it is usually done, so that the gain region is grown first and then the DBR. Once this has occurred, the DBR side is bonded to the heat spreader, and then the substrate is wet chemically etched. This requires an etch-stop layer to be grown on the respective end of the gain region to allow for controlled etching [5]. This has the benefit that heat spreader does not to be of optical quality, which saves on cost. However, the thermal properties of the DBR become important since it is between the heat spreader and the active region where heat primarily is generated. This is especially problematic when working with wavelength regimes where thick DBRs are necessary due to lack of available materials with a suitable refractive index contrast. This leads to the next strategy, the intracavity heat spreader. With an intracavity heat spreader, the active region itself is bonded to the heat spreader, so no chemical etching of the substrate needs to take place. This is better thermally, but more technically challenging in terms of bonding and the requirement for an optical quality heat spreader. These two strategies are illustrated below:

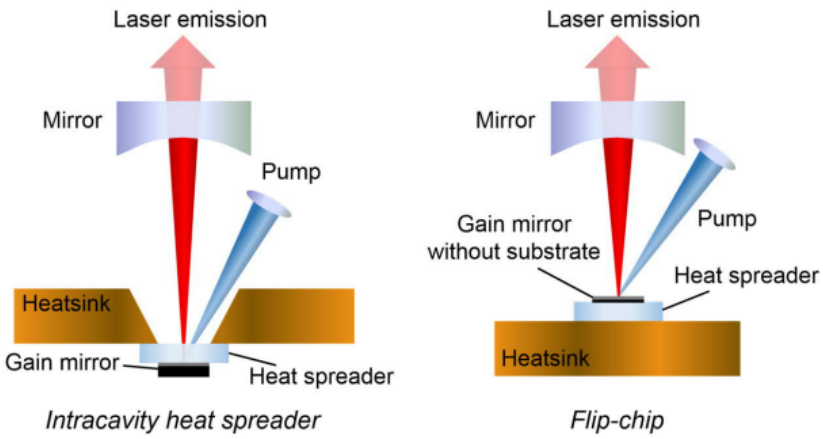

Figure 3.13. *Comparison of flip-chip intracavity heat spreader approaches. (Fig.from [28]).*

An additional strategy that has been explored is to combine both of these strategies and use two heat spreaders, one bonded directly to the active region such that it is an intracavity heatspreader, and the other bonded to the back side of the DBR as shown in the flip-chip strategy [29].

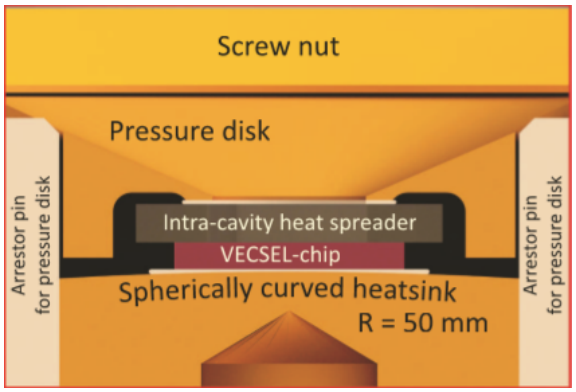

Figure 3.14. *3D-model of a two sided heat extraction method (Fig. from [29]).*

It is clear that thermal management of optically pumped semiconductor lasers is a key issue, and it is also clear that a DBR impairs the thermal behavior. This problem naturally leads itself to a solution, which is to simply remove the DBR. This seemingly obvious conclusion is the underlying principle of the MECSEL, a *membrane* external-cavity surface-emitting laser, a laser that is a thin slice of semiconductor material that is surrounded by bonded to intracavity heat spreaders on both sides. Besides thermal extraction, the lack of a DBR offers additional benefits ranging from improved mode locking, double-side pumping, a broader effective gain curve, and access to wavelengths not accessible with DBR limited VECSELs.

3.6 MECSELs

It is likely that more than one individual was working on the idea of DBR free operation but the first instance of the MECSEL concept being simulated was in 2013 [30]. Furthermore, the creation of a MECSEL was attempted in 2015 [7], achieved with a single heatspreader also in 2016 [31], and demonstrated with two heat spreaders in 2016 [8]. This will be the end of the "background" as the author sees further advancements as branching out from these starting points, and as such will be explored more in the outlook section. A schematic of Yang's and Kahle et al.'s design can be seen here:

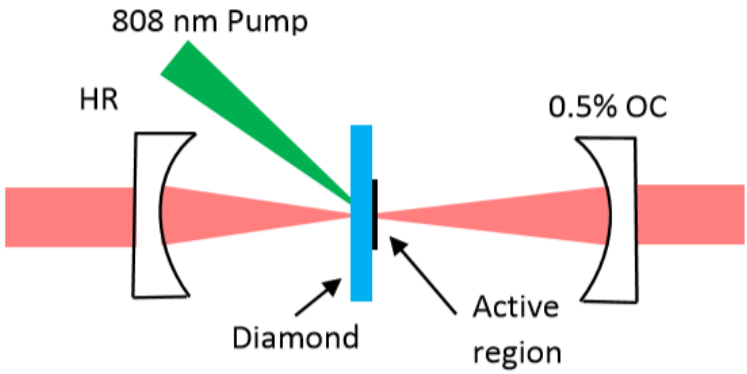

Figure 3.15. *Semiconductor disk laser with a single heatspreader (Fig. from Yang [32]).*

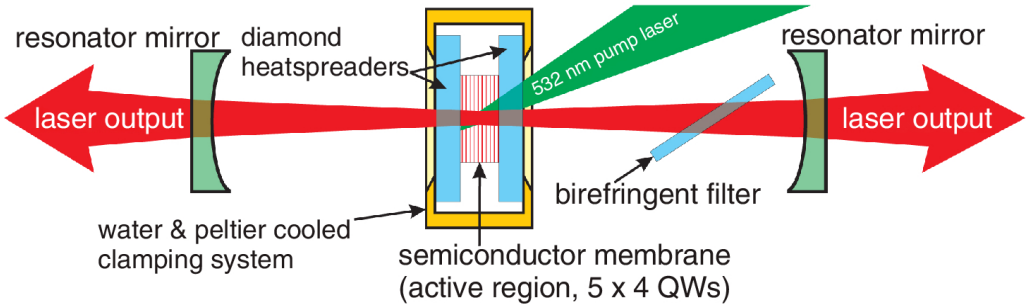

Figure 3.16. *MECSEL with two diamond heat spreaders (Fig. from Kahle et al. [8]).*

The motivation for creating a MECSEL was largely based on optimizing thermal management. This can be seen in the transition from initial improvements to VECSEL designs, such as flip-chip and the use of an intracavity heat spreader, and then to removing the DBR, and finally to a membrane with two heat spreaders. Differences in thermal extraction can be seen as a lower rise in temperature within the gain region. The temperature rise for these different strategies has been illustrated by Phung [33] in her doctoral thesis:

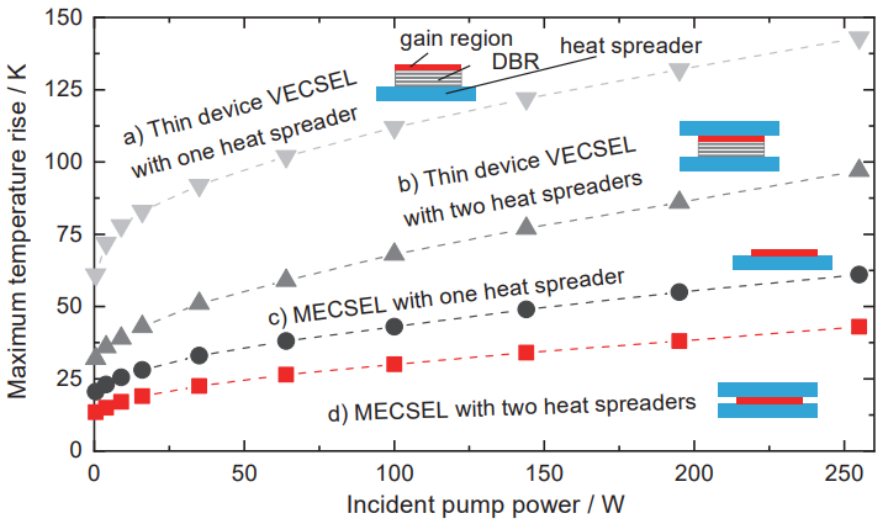

Figure 3.17. *Comparison of different heat spreader approaches, citations for each approach a[34], b[35], c[31], d[8] (Fig. from Phung [33]).*

The MECSEL approaches clearly outperform the other two VECSEL approaches.

3.7 Spectral Properties of MECSELs

As this thesis focuses on the tunable aspects, it is useful to look closer at the spectra of a MECSEL compared to a VECSEL. Before doing an experimental comparison, we can examine the theoretical "tuning" benefit of using a MECSEL compared to a VECSEL. As shown by Yang [31], having the end of the cavity, which in a VECSEL would be the attached DBR, farther away from the gain (the quantum wells), increases the gain bandwidth. The equation for integrated gain bandwidth is given by:

$$G(\lambda, z) = \int_0^L g(\lambda, z' - z) \sin^2\left[\frac{\pi m(\lambda) z'}{L}\right] dz' \tag{3.15}$$

where z can be varied and describes the position of the gain medium from the end of the cavity, λ also varies and is the wavelength in question, $g(\lambda, z)$ represents the longitudinal gain profile, L is the length of the cavity, and $m(\lambda)$ is the mode index which is equal to $\frac{2L}{\lambda}$. Additionally, as quantum wells are typically much smaller than the wavelength of light, an RPG structure with N quantum wells has a longitudinal mode profile approximated by:

$$g(\lambda, z) = G_0 \lambda \sum_N^{l=1} \delta\left[z - \frac{(l-1)\lambda_0}{2}\right] \tag{3.16}$$

where λ_0 is the RPG design wavelength, (remember that the spacing is in the peaks and troughs), $G_0(\lambda)$ is the gain for a single quantum well, and $\delta(z)$ denotes the Dirac delta function. Assuming the gain bandwidth for a single quantum well $G_0(\lambda)$ is spectrally flat such that $G_0(\lambda) = G_0$ and that lasing is occurring at the designed wavelength $\lambda = \lambda_0$ we can arrive at:

$$G(\lambda, z) = \frac{N}{2} G_0[1 + \mathrm{sinc}(N\pi\epsilon)\cos[(N - 1 + M)\pi\epsilon]] \tag{3.17}$$

where the distance of the gain membrane from the end mirror is $M = 4z/\lambda$ and normalized detuning is $\epsilon = (\lambda - \lambda_0)/\lambda_0$. Because of the difference in M between VECSELs and MECSELs since there is no DBR next to the gain medium, further simplifications can be made for each case. The bandwidth at full width at half maximum for a VECSEL is approximately $\Delta = \lambda_0/(2N)$ and for a MECSEL is approximately $\Delta = \lambda_0/N$. All of this math comes together to show that a MECSEL will give twice the structural gain bandwidth as a VECSEL along with a rapidly varying cosine component. This can be seen in the following graph adapted from Yang [32].

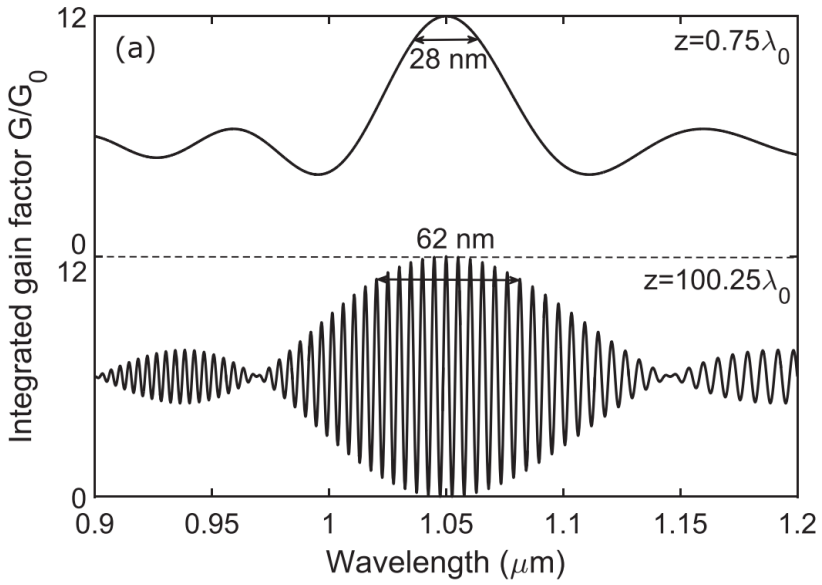

Figure 3.18. *Integrated gain for a $z = .75\lambda$ (top) and $z = 100.25\lambda$ (bottom) medium consisting of 12 quantum wells. At 90% of the maximum integrated gain, bandwidths of 28 nm and 62 nm are observed. (Fig. from Yang [31]).*

This difference can be seen experimentally instead of theoretically in the work of Kahle et al. where a similar gain region either had a DBR or external cavity mirror:

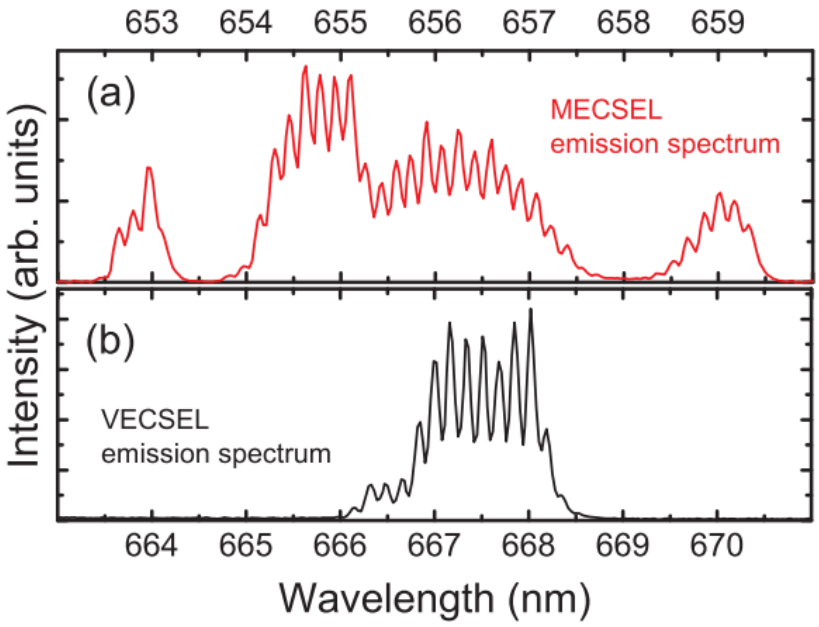

Figure 3.19. *Comparison of VECSEL and MECSEL emission spectra (Fig. from Kahle et al. [8]).*

This image contains multiple different effects. First, the diamond heat spreader/s used in this MECSEL/VECSEL create Fabry-Perot oscillations, which are calculated by the authors to be approximately 0.16 nm. This difference between peaks is called the free spectral range, or $\Delta\lambda$. The free spectral range is more often given in $\Delta\nu$ since this value will always be true, but the $\Delta\lambda$ requires a central wavelength, and even then is only accurate in the neighborhood of that central wavelength. The free spectral range is given by:

$$\Delta\nu = \frac{2}{n_g L} \tag{3.18}$$

where L is the length of the cavity, and n_g is the group index of the material. The group index is a more complete way at looking at refractive index, because it describes how the refractive index depends on the corresponding wavelength. Given a heat spreader thickness of 550 μm, central wavelength of around 667 nm, and refractive index of diamond at this wavelength regime to be around 2.41, this value indeed makes sense. For a fairly small tuning range, it can be assumed to be equal to the refractive index of the central wavelength. The other effect the authors describe is the beat note from the slightly different size of heat spreaders, which creates the larger pattern of dips and rises. While this can be avoided with the use of angled heat spreaders, this illustrates a few of the many technical considerations when optimizing MECSELs as tunable sources.

After the MECSEL was developed, work has been done by a few universities (and now companies!) around the world. The exploration of MECSELs as a tunable laser source narrows down the research to a very niche branch.

4 EXPERIMENTAL SETUP AND RESULTS

4.1 Experimental Methods

There are many steps in the process from going to a semiconductor wafer to a complete wafer structure. This thesis is primarily concerned with the performance of tunable MECSELs, so these steps will be covered in brief.

4.2 Growth

MECSELs can be grown by molecular beam epitaxy (MBE) as has been done by at the optoelectronics research center at Tampere University, or by metal organic vapor-phase deposition (MOVPE). These methods both work by taking a substrate wafer such as GaAs or InP and adding layers of atoms to it. This is done with effusion cells, where various substances are heated up to the temperature where sublimation takes place. These atomic shuttered evaporators are aimed at the substrate which is heated such that the impacting atoms have the mobility to find a suitable growth site. A schematic of an MBE chamber can be seen below:

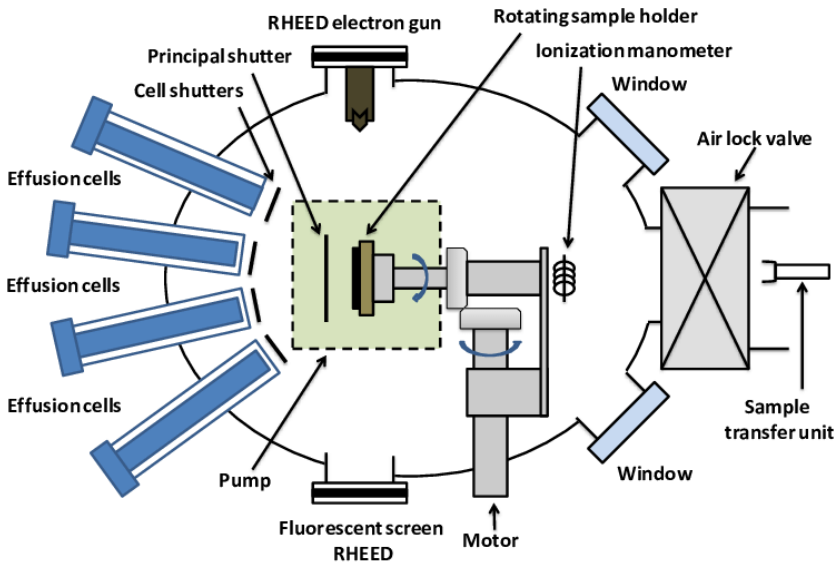

Figure 4.1. *A schematic of an MBE setup (figure from [36].*

Other factors like vacuum chamber temperature, pressure, shutter speed, substrate rotation, material impurities, and many others play a role in the accuracy and success of growth. MBE growth quality is a critical factor in the overall success of a laser.

Gain structures made with MBE in-house at Tampere University have been investigated by the author and the MECSEL team, leading to the author's bachelor's thesis [24] and many publications and presentations from Hermann Kahle, Hoy-My Phung and Philipp Tatar-Mathes. However, semiconductor lifetime constraints led us to switch to structures grown via MOVPE. The main difference between these two methods is that MOVPE is a chemical, not physical reaction. As such, the chamber is not a vacuum but is operated at relatively low pressure. Semiconductor organic complexes are used to go from gas phase and deposit the given material. For example, if GaAs is intended to be grown, trimethylgallium and arsine could be used. There are various pros and cons of these two growth strategies but exploring these differences is outside the scope of this thesis.

4.3 Semiconductor Characterization

After MBE or MOVPE growth, various tools like x-ray diffraction and electron diffraction can be used to measure the thickness and surface quality of the resulting semiconductor. Both of these tools rely on the diffraction of their respective particles by the semiconductor lattice. With the use of the Bragg condition for the crystal, constructive interference from the atomic layers gives information on the thickness and other properties of the semiconductor.

Another key tool for initial characterization is photoluminescence (PL). This technique involves shining a laser (typically) with a shorter wavelength on the semiconductor and measuring the emitted light. Vertically emitted or edge emitted light can be collected for PL measurements, though slight differences between the two do exist. Initially, a PL map is taken of the entire wafer after growth. The purpose of this measurement is to allow for the selection of the best-performing parts of the wafer to be used in the MECSEL, as there is a large amount of variation in wafer quality in different parts of it. While these pre-characterizations were not taken as the samples were grown elsewhere, an example from another structure that was grown in-house is given by Phung [33]:

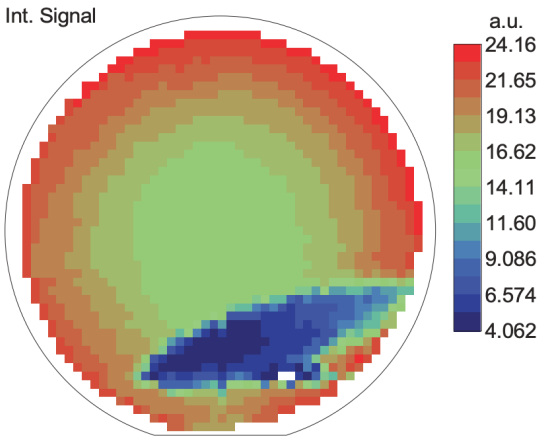

Figure 4.2. *A PL map with intensity given in arbitrary units. Discounting the edges of the wafer, it can be seen the middle has strong intensity while a spot towards the bottom has weaker intensity. [36].*

where a.u. stands for arbitrary units. Considering this map, it would make sense to use a slice from the middle of the wafer for incorporation in a MECSEL.

Additionally, the spectral information from a PL mapping measurement can give information on the expected lasing wavelength. A spectral tuning measurement of a MECSEL taken with a PL setup created by Rantaniemi [37] is as follows:

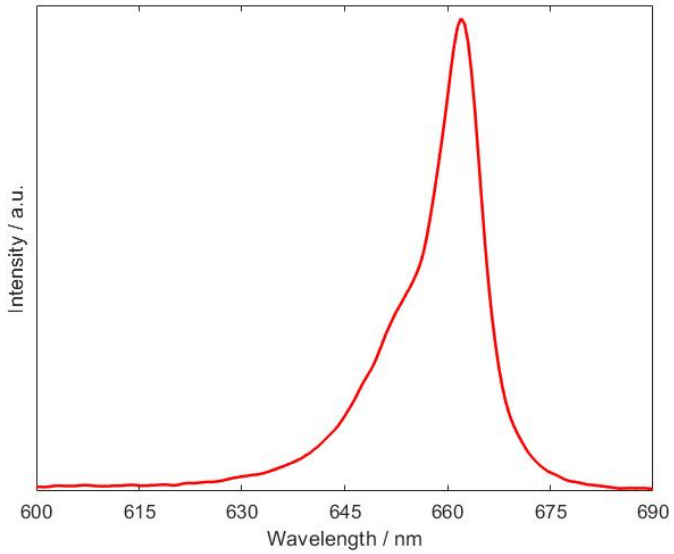

Figure 4.3. *A vertical PL curve from a cleaved MECSEL sample. Image and data from [37].*

This spectral information is not a perfect correlation with the lasing wavelength, but that information can be predicted from previous similar samples and with the general rule that the lasing wavelength is slightly redshifted compared to the PL peak wavelength. The comparison of intensity between different samples is also a useful tool to determine

which will perform the best.

4.4 Wafer Processing and Bonding

After MBE or MOVPE, the finished product is a circular wafer. If the MECSEL is made in certain MBE growing conditions, rapid temperature annealing (RTA) would take place to improve crystal quality. RTA consists of heating up the wafer (with a protective layer on it) for a short period of time which depends on the parameters of the semiconductor structure. This process is repeated until the sample is properly cured. Progress can be measured via PL intensity comparison. Wafer pieces are then diced into approximately 8 mm squares either manually with a scribe or with a dicing saw. The next step is heat spreader bonding. Three different heat spreader materials have been used to the author's knowledge for MECSELs, namely sapphire, silicon carbide (SiC), and diamond. Both diamond and SiC heat spreaders were used in this thesis and are described in more detail.

It is important to realize the strengths and weaknesses of each material. Starting with SiC, it is quite cheap and achieves good bonding with the bonding procedure used. SiC also does not suffer from the birefringence that is common in diamond. Diamond makes up for its lacking optical quality with superior thermal conductivity. Diamond is often coated with dielectric anti-reflection coating to reduce lost pump and cavity light, but especially reduce the etalon effect caused be heat spreaders. A comparison of the shows that diamond has a thermal conductivity of 20 $\frac{\mathrm{W}}{\mathrm{cm\,K}}$ while SiC has a thermal conductivity of around 3.7 $\frac{\mathrm{W}}{\mathrm{cm\,K}}$ [38]. The improved thermal conductivity that diamond provides raises the maximum power which can be used to pump a MECSEL and means that the input power to output power curve will be higher, giving increased efficiency at high power. However, there is the drawback that diamond is currently very difficult to grow with high optical quality, leading to potentially prohibitive prices for the highest quality options. The corresponding situation is such that both choices of heat spreader are interesting from a research and potentially industrial setting as seen in Thorlabs Crystalline Solutions [39]. A comparison between the performance of diamond vs. SiC heat spreaders was explored in the author's bachelor's thesis as seen in Fig. 4.4.

Before any bonding can take place, the wafer and heat spreaders need to be cleaned, which is done chemically in an ultrasonic bath. Then, the active region side of the wafer is bonded to a heat spreader with a larger area than the wafer slice. The substrate is then wet chemically etched away. This is done by dipping the sample in a solution of ammonium hydroxide/hydrogen peroxide for a time determined by wafer thickness. This process leaves an etch stop layer on top of the active region, which is removed by a quick dip in hydrofluoric acid. This would damage the gain material itself if not for the cap layer that is resistant to the hydrofluoric acid due to low aluminum content. The second heat spreader can be bonded after the substrate and sacrificial layers are removed. Achieving successful bondage of the heat spreaders and semiconductor structure is a crucial step in

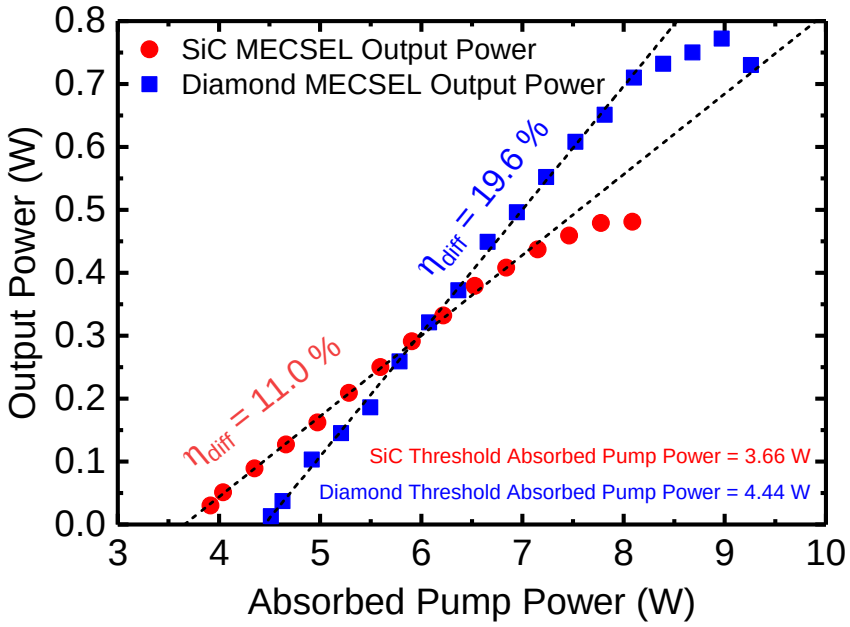

Figure 4.4. *Comparison of a MECSEL with a SiC heat spreader and an anti-reflection coated (for the pump laser and the MECSEL wavelength) diamond heat spreader (Figure and text from [24].*

creating a working device. Wafer bonding is a critical aspect in many semiconductor fields and new strategies are being explored by groups such as Thorlabs Crystalline Solutions [39]

4.5 MECSEL Cavity and Holder

When the MECSEL chip is ready to be implemented in a laser, the MECSEL is glued to a copper mount custom designed by Hermann Kahle that allows for water cooling close to the membrane. This mount is constructed by two copper plates with a lifted hole in the middle for the MECSEL. This construction is situated within an aluminum tube and glued in place such that the system is water-tight. If one is familiar with this type of bonding, it should be noted that this method did not involve using indium foil, as it was found to not be necessary with clever design and careful gluing. However, this is by no means the perfect strategy for bonding in terms of both difficulty and thermal conductivity. This mount is hooked up to a water chiller, allowing for both controlled room temperature operation and experimentation at other temperatures. This is particularly useful for measuring the thermal resistance of a MECSEL, which requires evaluating the change in wavelength when the temperature of the heatsink is varied. This entire structure is then placed on a 5-axis mount for easy customization and optimization.

4.6 MECSEL Cavity

The MECSEL cavity used for most of the experiments in this thesis consists of the MECSEL chip (both active region and heat spreaders) and mount, external mirrors in a linear

or v-shape configuration, double-side pumping optics, and a birefringent filter for tuning. A schematic of this setup with double-side pumping is given in Fig 4.5.

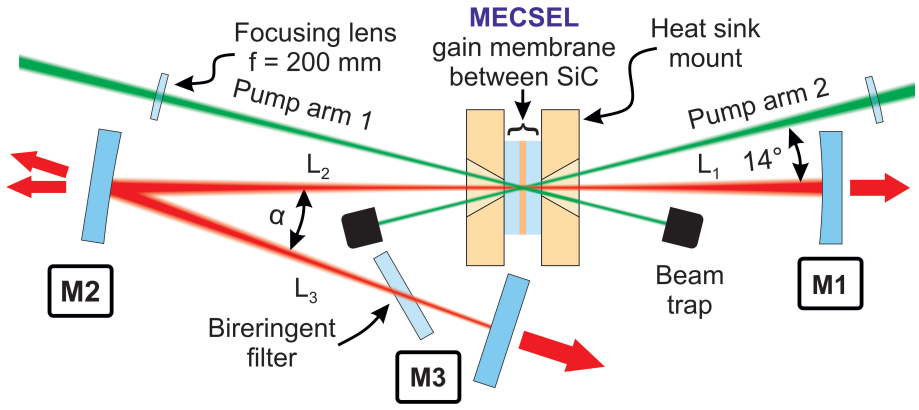

Figure 4.5. *MECSEL operating in a V-shape cavity with a birefringent filter. Image created by Hermann Kahle.*

A coherent Verdi-6 was used as a pump source. This pump laser consists of two bars of semiconductor diode lasers operating at 808 nm which pump a Nd:YAG laser operating at 1064 nm, which is then frequency doubled to 532 nm. This strategy is commonly used for the pumping of Ti:Sa lasers, as they have an absorption maximum near 532 nm. While we used this high quality pump beam, MECSELs and similar lasers are capable of using low quality beams which will be touched on in the outlook. The power provided by this pump is insufficient for power scaling MECSELs, especially samples with diamond heat spreaders and/or when using a large pump spot. The pump beam first passes through an adjustable half-wave plate, allowing manipulation of the beam's polarization. This modulated beam is then split with a polarizing beam splitter. The benefit of using a polarizing beam splitter is two-fold. First, by changing the rotation of the half-wave plate, the percentage of beam intensity in each arm can be adjusted. This is useful using an asymmetrical quantum well design or heat spreaders with non-equal reflectivities. Secondly, the polarizing beam splitter provides orthogonally polarized beams for pumping which avoids constructive and destructive interference where the beams converge in the MECSEL. Once split, each beam is focused with the use of a plano-convex lens. The size of the pump spot can be adjusted by moving the focusing lens closer or farther away from its focal distance. The pumps are at an angle to avoid being in the intracavity beam path and general practicality. This angle is kept small, around 14 degrees to avoid significant beam ellipticity.

Two very similar, but different membrane structures were investigated in this thesis. One contains five quantum wells, and the other contains ten quantum wells.

4.7 Application Specific Criteria

One of the target applications when designing these tunable MECSELs was optical coherence tomography (OCT). This measurement strategy is a non-invasive imaging modality that lies between ultrasound and microscopy in resolution and allows for real-time 3-D

cross-sections of biological tissues and systems [40]. This is possible by measuring the light reflected from tissue, and by using the coherence and varying wavelength (or spectral broadness) of the source, creating a scan. The state-of-the-art light source for OCT is the Ti:Sa laser but the MECSEL could solve two issues given in this laser type. The first is price, which has been covered in the application context, and the second is the wavelength range in which a MECSEL can operate. A MECSEL can operate at shorter wavelengths than a conventional Ti:Sa, a fact that is relevant based on the absorption spectra of water. This is illustrated in Fig 4.6.

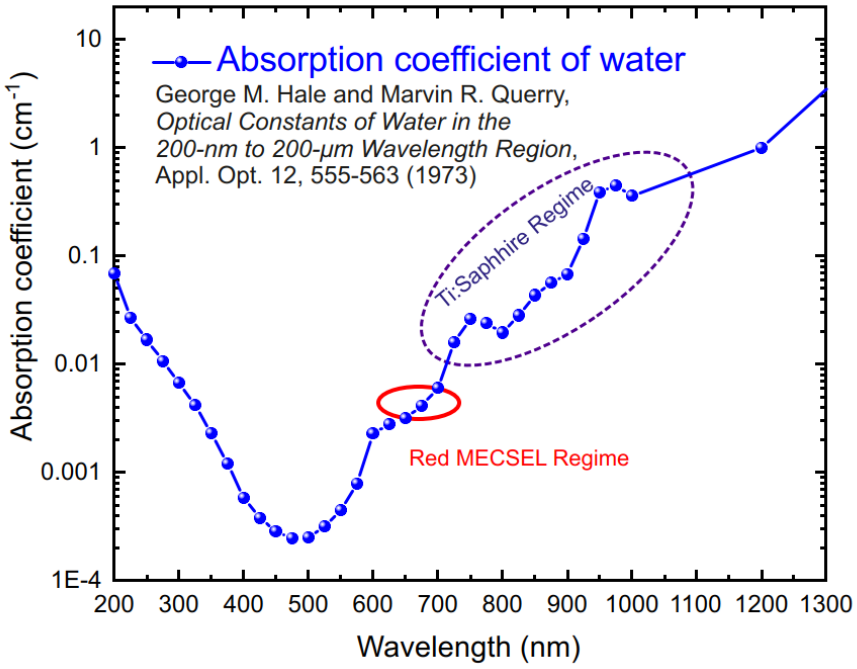

Figure 4.6. *Absorption coefficient of water with varying wavelength showing MECSEL and Ti:Sa tuning regimes. Source of data given in the image. Graph made by Philipp Tatar-Mathes and adapted by the author.*

As can be seen, there is roughly a 10x difference in the absorption coefficient in the red MECSEL tuning regime compared to the Ti:Sa regime. Resolution is an important factor in OCT, and the axial resolution is given by:

$$\Delta z = 0.44 \frac{\lambda_0^2}{\Delta\lambda} \tag{4.1}$$

where λ_0 is the central wavelength of the laser, and $\Delta\lambda$ is the tuning range. With this in mind, a laser with a broad tuning range and relatively short wavelength would be optimal for OCT. Another consideration is the linewidth of the laser source. Linewidth refers to the spectral full-width at half maximum. The range at which OCT measurement is possible is given by:

$$\Delta z = \frac{2\ln(2)}{\pi} \frac{\lambda_0^2}{\delta\lambda} \tag{4.2}$$

However, there are other spectral properties that are desired, such as "continuous" tunability, meaning that the wavelength peaks are very close together. This is a challenging aspect due to the etalon effect that is present because of heat spreaders and the MECSEL membrane itself. While anti-reflection coatings certainly help, the etalon effect remains. Etalon effects are discussed in the following sections.

4.8 Tools for Tuning

Tuning was achieved with an intracavity birefringent filter as shown in Fig. 4.5. The birefringent filter is inserted at Brewster's angle such that there is no reflection of p-polarized light. Brewster's angle is given by Brewster's law:

$$\theta_B = \arctan \frac{n_2}{n_1} \tag{4.3}$$

where θ_B is Brewster's angle, n_2 is the refractive index of the second material (the filter) and n_1 is the refractive index of air and is approximately equal to one. Increasing the thickness of the birefringent filter results in a reduced free spectral range as well as additional losses. As the filter is aligned by hand, this angle is found by maximizing the intensity of the laser passing through it, as this occurs at Brewster's angle. The filter is then rotated, which then gives wavelength-dependent losses and acts as a means of mode selection.

An etalon can also be inserted into the cavity. The heat spreaders present in the cavity already act as intracavity etalons, so it may seem counterproductive to include an additional etalon. However, the behavior of multiple etalons is complex [41] and have to be modeled, which was done with LightMachinery software [42]. An example of the transmission spectrum of the combination of a 1 mm YAG etalon (40% reflectivity) and two quartz -to simulate diamond- heat spreaders (1% reflectivity) can be seen in Fig. 4.7. One quartz etalon has a thickness of 0.51 mm to demonstrate how small variations in thickness can affect the transmission spectra.

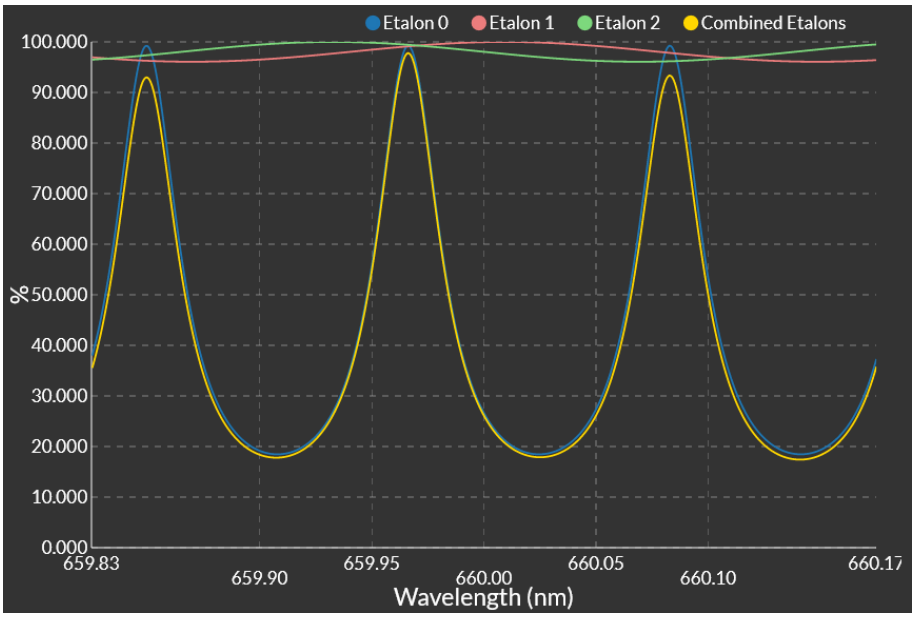

Figure 4.7. *Transmission spectra of three etalons using LightMachinery software [42].*

A general principle for etalons is that the higher reflectivity of the surfaces, the narrower linewidth. Additionally, the smaller distance there is between the surfaces, the larger the free spectral range. While the transmission spectrum in this image is dominated by the higher reflectivity YAG etalon, this is not given in practice. Steps are taken to reduce the reflectivities of all interfaces, but any interface will have some amount of reflection, leading to an unavoidable etalon effect.

4.9 Tuning Experiment

The tuning range was first evaluated without an etalon, only a 2 mm birefringent filter. The shape of the tuning curve can be seen by performing a trial comprised of many individual measurements. In this trial the output power is stronger in certain regions compared to others with the more continuous information provided by the multitude of peaks. Spectral data can be seen in Fig. 4.8.

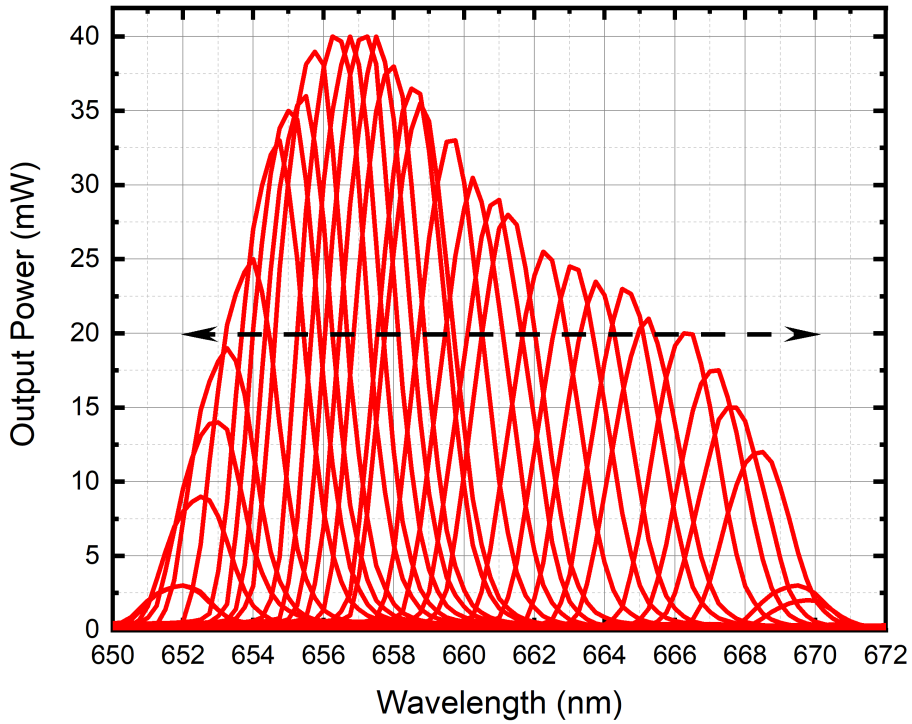

Figure 4.8. *Tuning curve of a 5x4 anti-reflection-coated diamond heat spreader MECSEL by Tatar-Mathes, Koskinen, and the author.*

Etalon effects were first investigated, a MECSEL cavity was setup with a 1 mm YAG (Yttrium aluminium garnet crystal) etalon and 2 mm birefringent filter. The active region consisted of five packets of four quantum wells (5x4). Anti-reflection coated diamond heat spreaders were used to ensure a good thermal situation and to minimize heat spreader etalon effects. The cavity was put into a z-cavity to allow for easier alignment. The method used for creating a z-cavity was to use two highly reflective curved mirrors and two planar flat mirrors where the two curved mirrors were at the top of the Z with the membrane in between them and the tuning elements in the lowest intracavity space. This can be seen in the following picture of the z-cavity setup with a birefringent filter and etalon:

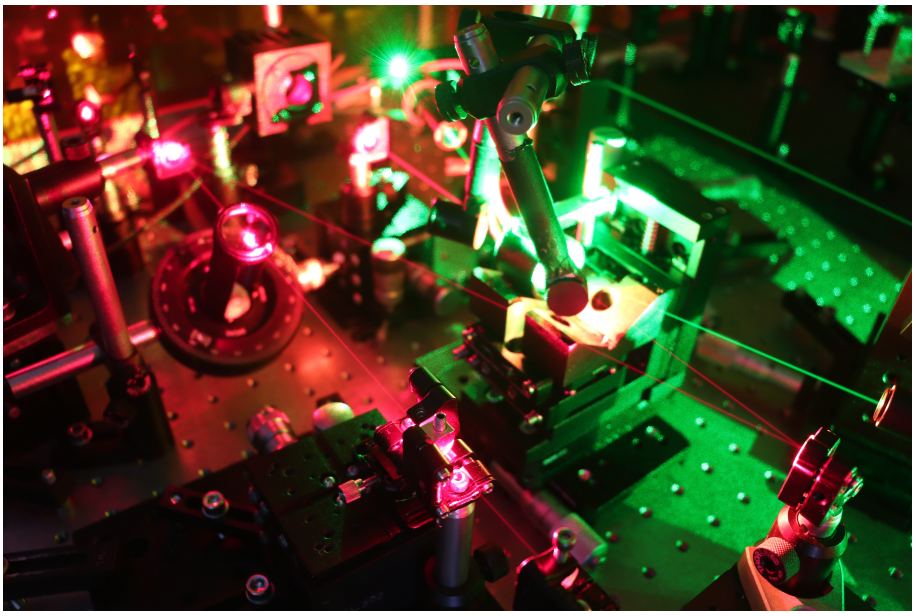

Figure 4.9. *Lab setup of a z-cavity containing a birefringent filter and intracavity etalon. Photo credit Hermann Kahle.*

The water cooling temperature was set to 10°C to ensure maximum performance. The sample was double-side pumped with a total of 6.5 W. A tuning range was measured with an optical spectrum analyzer in coordination with a power meter and can be seen in Fig. 4.10.

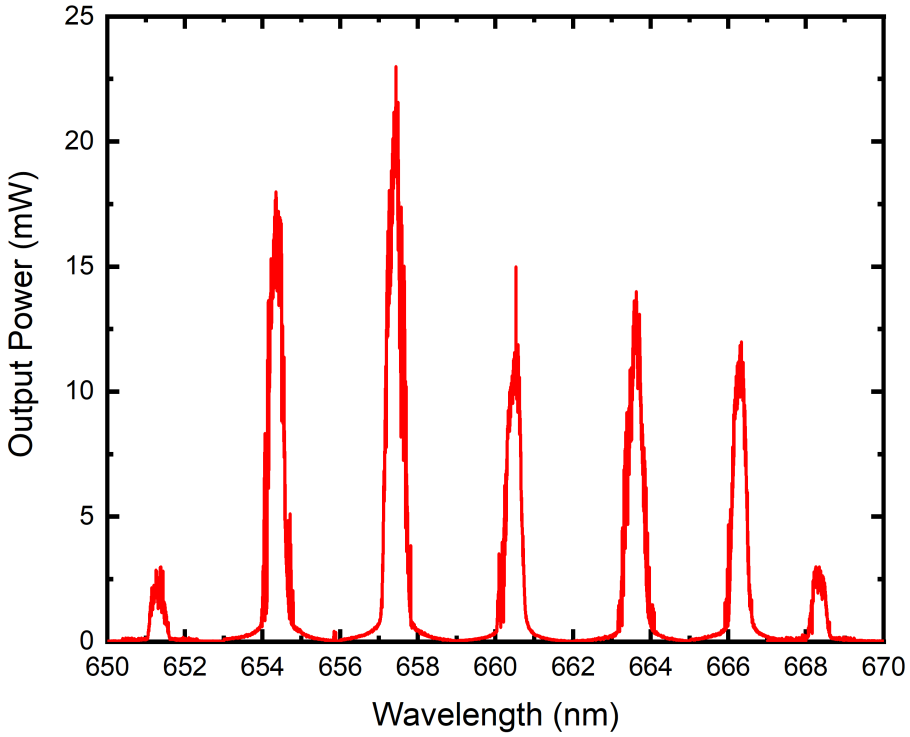

Figure 4.10. *Tuning curve of 5x4 anti-reflection-coated diamond MECSEL with the corresponding output power.*

The intention of the etalon was to get a narrower, but continuous linewidth, and in this instance a linewidth of around 0.67 nm was obtained using Gaussian analysis.

A different configuration was attempted with a 10x4 MECSEL. Instead of a z-cavity, this MECSEL was inserted into a v-cavity. Additionally, a highly reflective etalon (R=97%) was used as a back mirror and outcoupler. This sample was also double-side pumped with 6.5 W of total power, but a warmer chiller temperature of 18°C was used to obtain more realistic results. The etalon used was 1 mm thick fused silicon and the spectra were collected from the light passing through the backside of this etalon. As with the previous measurement, a 2 mm birefringent filter was used for tuning. The spectra can be seen in Fig. 4.11.

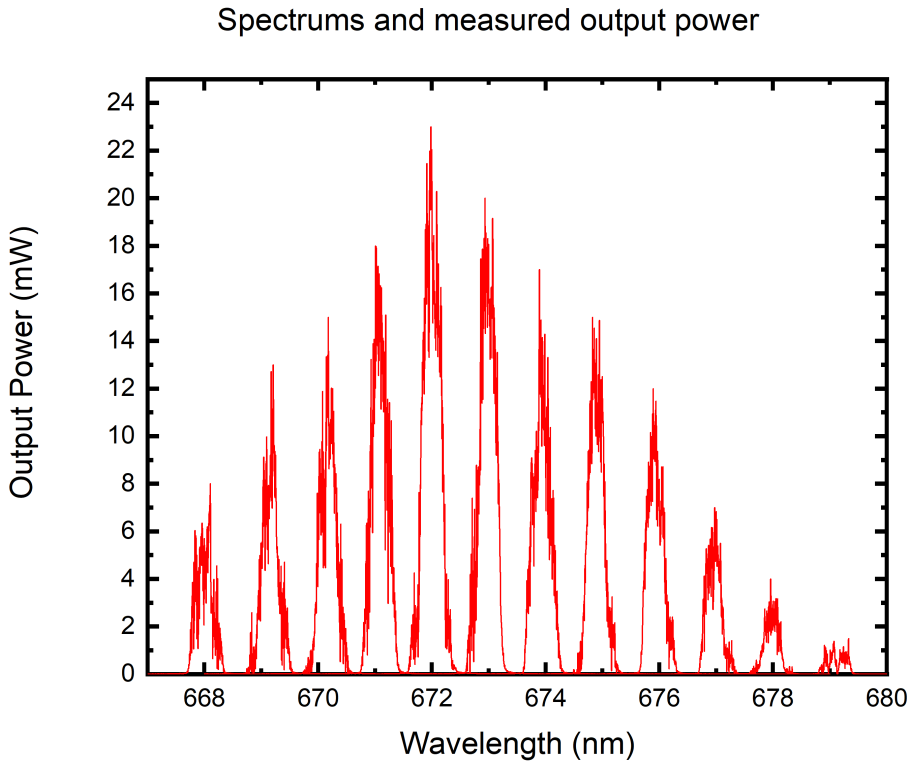

Figure 4.11. *Spectra from 10x4 MECSEL with uncoated diamond heat spreaders.*

It is useful to note that for a target application like OCT, around 5 mW of output power is required, so the "useful" tuning range for this trial is around 9 nm as deducted from Fig. 4.11. The most important distinctions between this and the previous trial are the higher reflection etalon and the uncoated heat spreaders. A higher reflection etalon should give a narrower linewidth, and this principle holds true as this trial with the 97% reflectivity etalon has an average linewidth of approximately 0.35 nm compared to the previous trial with approximately 0.67 nm. This may be compounded by the increase in heat spreader reflectivity.

When looking closely at the peaks in Fig. 4.11 it is clear that there are many competing modes operating simultaneously and that a simple Gaussian peak is not present. The

resolution of the optical spectrometer used for the measurements so far was 0.05 nm and to study the spectra further a higher resolution spectrometer with a resolution of 0.01 nm was used. A 10x4 MECSEL with 40% reflectivity coated diamond heat spreaders was measured with a 0.01 nm optical spectrum analyzer, first with only the etalon and no birefringent filter. The 10x4 structure was investigated as it theoretically should outperform the 5x4 structure. However, the experimental results did not support this conclusion. Twenty averages were taken to reduce noise from random fluctuations. This gives a very wide spectrum as seen in Fig. 4.12.

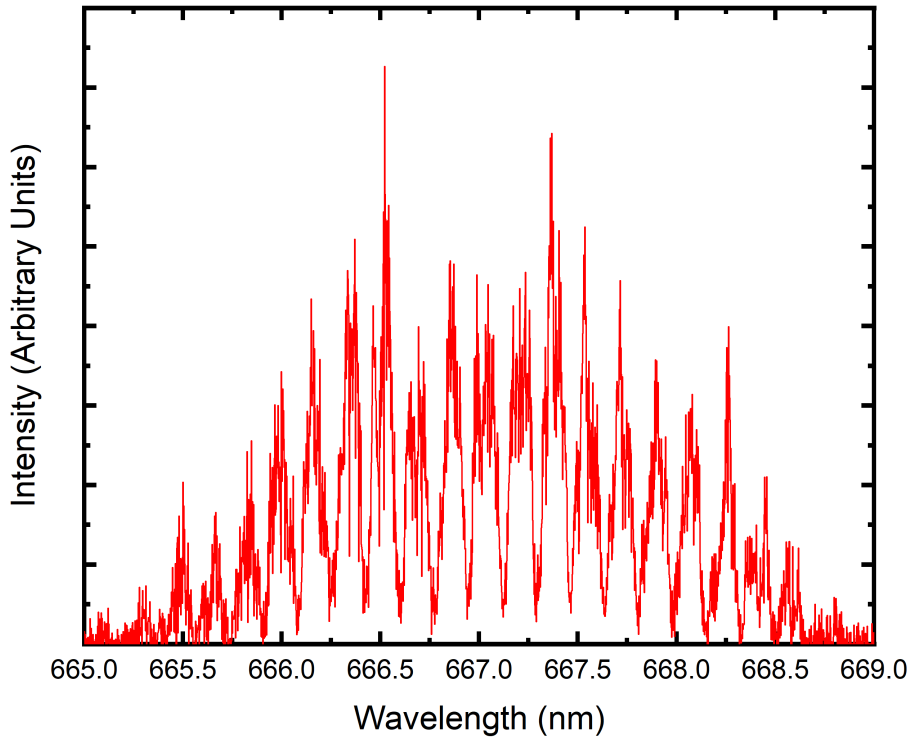

Figure 4.12. *Averaged spectra from a 10x4 MECSEL with no birefringent filter showing broadband emission.*

The free spectral range was estimated with this graph to be around 0.16 nm. However, it is difficult to know if this is truly the free spectral range or a macro-pattern containing micro-patterns. A high resolution spectrum was captured with a 2 mm birefringent filter inserted into the cavity, giving a near single peak. This high-resolution peak, taken with 20 averages, can be seen in Fig. 4.13.

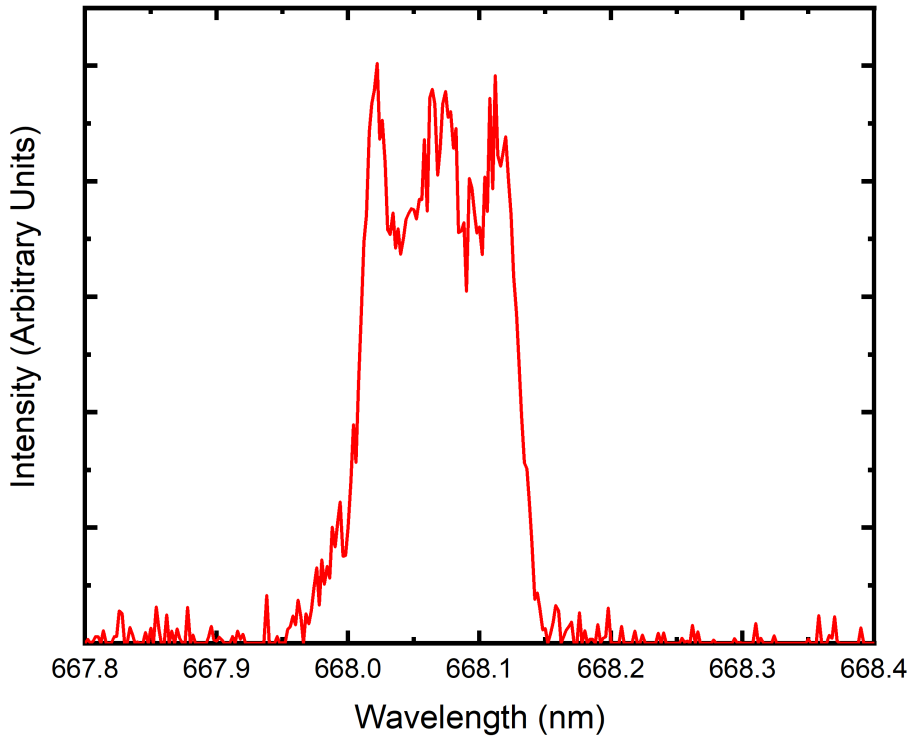

Figure 4.13. *Averaged spectra from a 10x4 MECSEL with birefringent filter showing tuning emission.*

A clean Gaussian profile is not obtained. Multiple spectra were taken without averaging and without moving the birefringent filter, such that the exact same peak should be observed. These peaks were sharper, but moved around slightly in the wavelength domain, suggesting that the exact peak location is fluctuating with time. This would explain why Fig. 4.13 has a more broad, non-Gaussian shape, as multiple modes are present and fluctuate with time. Solutions for this instability were discussed within the MECSEL team, and it was agreed upon that laser active frequency stabilization [43] would be required. Active frequency stabilization is complex and requires expertise in the area, therefore representing the next step forward in allowing MECSELs to be used for numerous applications.

5 CONCLUSION

This thesis looked at ways to expand the MECSEL concept for use as a tunable, high-power, diffraction-limited light source. Tuning with multiple structures was investigated and novel cavity designs and intracavity elements were explored. The results were not record-setting in themselves, but highlight paths forward and especially show the limitations that need to be overcome. The main challenge that is set forward is the creation of an actively frequency-stabilized MECSEL. Additionally, Etalon effects could also be addressed with the use of wedged heat spreaders. The rest of the outlook will examine the current state of MECSELs, both in research and industry.

5.1 Research at Tampere University

One strategy to make MECSELs more attractive is to demonstrate pumping with green laser diodes. MECSELs in the infrared are commonly pumped with laser diodes [44], as powerful diodes are available at these wavelengths. However, green diodes with watt-level power are new to the market, and to the author's knowledge have not been documented as pump sources for a MECSEL or VECSEL. Creating a setup where diodes are combined together in a fiber with a small enough beam diameter is technically challenging and has been explored by Antti Rantaniemi in unpublished work. It seems likely that green diode technology will advance further, and eventually make its way to be a much cheaper power source for optically pumped semiconductor lasers. This is a key advantage that optically pumped semiconductor lasers have over Ti:Sa lasers and could provide a market sector as MECSELs and similar lasers continue to be improved.

Another benefit that MECSELs can exploit is the use of different quantum wells. This was explored by the MECSEL team at Tampere University (including the author) in trials where quantum wells corresponding to lasing at 720 nm, 740nm, and 760nm were grown monolithically and made into a MECSEL. Unfortunately, cracking due to growth issues left this experiment with disappointing results. However, this idea is being further explored by Rajala, also at Tampere University in unpublished work.

5.2 Research Elsewhere

MECSEL technology continues to be explored by a few research teams, and more recently by two companies. A by no means exhaustive view into neoteric research could

start with a team in Poland investigating long wavelength MECSELs. These MECSELs are grown on indium phosphide and have been demonstrated with wavelengths such as 1750 nm [45] and 1600 nm [46]. This team seems to have an emphasis on epitaxy, such that various growth parameters and measurements can be seen throughout their papers. There have not been any MECSEL papers published by this team since 2020 so it seems possible their MECSEL project has ended.

The well-known professor Ursula Keller is responsible for work somewhat related to the concept, one example [47] being the MIXSEL (mode-locked integrated eternal-cavity surface-emitting laser). This basically consists of a VECSEL with an integrated SESAM (semiconductor saturable absorbing mirror). A SESAM is normally a separate mirror that is used for modelocking, but this research shows that it can be integrated which increases cavity simplicity.

MECSELs continue to be explored at both Stuttgart University and the University of Southampton as seen their collaborations [48]. However, the interest in MECSELs in Southampton seems to be a facet of their ongoing work with VECSELs and the research at Stuttgart appears to be the remaining interest that did not get transferred to their spinoff 21 Semiconductors.

Prof. Mansoor Sheik-Bahae and his team at the University of New Mexico have investigated mode-locking [49], high power IR emission for frequency doubling [50], and hybrid MECSELs also in the same paper [50]. A hybrid MECSEL is where a DBR is used, but it is bonded to the outside of the heat spreader so that the structure can still benefit from improved thermal extraction. They are targeting this wavelength specifically for frequency doubling to 589 nm for use as a guide star, which is a ground-based telescope tool for measuring atmospheric fluctuations by exciting sodium ions high up in the atmosphere. This group is also involved in wafer scale manufacturing [39] in collaboration with California-based Thorlabs Crystalline Solutions and with German-based 21 Semiconductors.

Wafer scale manufacturing is a key part of 21 Semiconductors' main product that they've called a MEXL (Membrane eXternal cavity laser). The MEXL is a customizable compact gain and heat spreader chip designed to be frequency doubled to the yellow/yellow-green wavelength range. The choice of name is interesting, as the "coiner" of the MECSEL name and also one of the supervisors of the author, Hermann Kahle, is a previous coworker with many of the 21 Semiconductors team at Universität Stuttgart and is mentioned on their website, so they clearly know of the MECSEL term (in fact a diagram of a MECSEL is described with that terminology on their site). Looking at the difference in the acronym, the phrase "surface-emitting" is missing from the acronym MEXL, but their device very much appears to be a surface emitter. This suggests that either their device has some other key difference that is not described on the website, or that they wanted to differentiate their product or simply thought MEXL would be better in terms of marketing. Intellectual property concerns could also be a reason. Their product appears to be highly developed and made for integration with preexisting laser systems.

Thorlabs Crystalline Solutions is a bit harder to get information about, as this was originally a company called Crystalline Mirror Solutions that was bought by Thorlabs. The Thorlabs site has information on their current product line of low noise and thermally conductive mirrors, which makes sense considering these mirrors consist of "Single-Crystal GaAs/AlGaAs Optical Coatings", suggesting they are DBRs wafer bonded to various substrates. Given the lack of public information, I decided to reach out to Garrett Cole, a cofounder of Crystalline Mirror Solutions and technology manager at Thorlabs Crystalline Solutions, who was kind enough to answer some questions I had about the company. Specifically, their bonding is indeed done on the whole wafer scale, where plasma activation followed by annealing is used as a bonding method. They normally use SiC as a heat spreader material, and when asked about the potential for diamond as a heat spreader material, Cole explained, "We have had very poor yield with both **censored** and **censored** single-crystal diamond substrates. At this point in time I would skip that unless you have a very promising diamond supplier." From conversations with the MECSEL team at Tampere University, it has been clear that even finding and purchasing very small high quality diamonds is difficult, so it is not hard to imagine that wafer size diamond substrates are not at the required quality with current CVD diamond growth technology. If this technology progresses to the point where wafer scale diamonds are both more affordable and of high quality, this would make for an excellent substrate material and would likely be integrated by both 21 Semiconductors and Thorlabs Crystalline Solutions given a need for high performance devices.

In conclusion, MECSELs continue to be investigated by a small group of researchers and has recently made its way into the world of industry. While the laser guide star use case is an application being explored, the MECSEL is for the most part a laser solution looking for its problem.

REFERENCES

[1] Sorkin, P. and Lankard, J. Stimulated emission observed from an organic dye, chloro-aluminum phthalocyanine. *IBM J. Res. Develop* 10 (1966), 162–163. DOI: 10.1147/rd.102.0162.

[2] Schäfer, F. P., Schmidt, W. and Volze, J. Organic Dye Solution Laser. *Applied Phys. Lett.* 9 (1966), 306–309. DOI: 10.1063/1.1754762.

[3] Duarte, F. Organic Dye Lasers: Brief History and Recent Developments. *Optics and Photonics News* 14 (2003), 20–25. DOI: 10.1364/OPN.14.10.000020.

[4] Moulton, P. F. Spectroscopic and laser characteristics of Ti:Al2O3. 3:1 (Jan. 1986). DOI: 10.1364/JOSAB.3.000125.

[5] Kuznetsov, M., Hakimi, F., Sprague, R. and Mooradian, A. High-power (>0.5-W CW) diode-pumped vertical-external-cavity surface-emitting semiconductor lasers with circular TEM_{00} beams. *IEEE Photonics Technology Letters* 9.8 (1997), 1063–1065. DOI: 10.1109/68.605500.

[6] O. Okhotnikov and *et al.*, eds. *Semiconductor Disk Lasers: Physics and Technology*. Wiley-VCH, 2010.

[7] Jones, B. ZnCdMgSe and AlGaInP multi-quantum well films for colour conversion and optically-pumped visible lasers. PhD thesis. 2015.

[8] Kahle, H., Mateo, C. M. N., Brauch, U., Tatar-Mathes, P., Bek, R., Jetter, M., Graf, T. and Michler, P. Semiconductor membrane external-cavity surface-emitting laser (MECSEL). *Optica* 3.12 (2016), 1506–1512. DOI: 10.1364/OPTICA.3.001506.

[9] Gordon, J. P., Zeiger, H. J. and Townes, C. H. The Maser—New Type of Microwave Amplifier, Frequency Standard, and Spectrometer. *Physical Review* 99 (4 1955), 1264–1274. DOI: 10.1103/PhysRev.99.1264.

[10] Maiman, T. Stimulated Optical Radiation in Ruby. *Nature* 187 (1960), 493.

[11] Javan, A., Bennett, W. R. and Herriott, D. R. Population Inversion and Continuous Optical Maser Oscillation in a Gas Discharge Containing a He-Ne Mixture. *Physical Review Letters* 6 (3 1961), 106–110. DOI: 10.1103/PhysRevLett.6.106.

[12] Hall, R. N., Fenner, G. E., Kingsley, J. D., Soltys, T. J. and Carlson, R. O. Coherent Light Emission From GaAs Junctions. *Physical Review Letters* 9 (9 1962), 366–368. DOI: 10.1103/PhysRevLett.9.366.

[13] *Britney Spears' Guide to Semiconductor Physics. Basic Semiconductor Physics*. Aug. 25, 2020. URL: http://britneyspears.ac/physics/fplasers/fplasers.htm.

[14] Basov, N., Bogdankevitch, O. and Grasuk, A. Semiconductor lasers with radiating mirrors. *IEEE Journal of Quantum Electronics* 2.4 (1966), 154–154. DOI: 10.1109/JQE.1966.1073948.

[15] Basov, N., Vul, B. M. and Popov, Y. M. Quantum-mechanical semiconductor generators and amplifiers of electromagnetic oscillations. *Journal of Experimental Theoretical Physics (U.S.S.R)* 37 (1959), 587–588.

[16] Kroemer, H. A proposed class of hetero-junction injection lasers. *Proceedings of the IEEE* 51.12 (1963), 1782–1783. DOI: 10.1109/PROC.1963.2706.

[17] Streetman, B. and Banerjee, S. *Solid State Electronic Devices*. Pearson, 2016.

[18] Fermi, E. *Nuclear Physics*. University of Chicago Press, 1950.

[19] *Laser concepts*. Apr. 2019. URL: https://www.21semiconductors.com/innovation/laser-concepts/.

[20] Iga, K., Koyama, F. and Kinoshita, S. Surface emitting semiconductor lasers. *IEEE Journal of Quantum Electronics* 24.9 (1988), 1845–1855. DOI: 10.1109/3.7126.

[21] URL: http://maxwellrules.com/meep/distributed_bragg_reflector.html.

[22] Soda, H., Motegi, Y. and Iga, K. GaInAsP/InP surface emitting injection lasers with short cavity length. *IEEE Journal of Quantum Electronics* 19.6 (1983), 1035–1041. DOI: 10.1109/JQE.1983.1072000.

[23] Kuznetsov, M. E. History of Optically Pumped Semiconductor Lasers – VECSELs. *Vertical External Cavity Surface Emitting Lasers*. John Wiley & Sons, Ltd, 2021. Chap. 1, 1–25. ISBN: 9783527807956. DOI: 10.1002/9783527807956.ch1.

[24] Rogers, A. Setup and Characterization of Emission Properties of a Red-Emitting MECSEL. PhD thesis. 2021. URL: https://urn.fi/URN:NBN:fi:tuni-202104273933.

[25] Heinen, B., Wang, T., Sparenberg, M., Weber, A., Kunert, B., Hader, J., Koch, S., Moloney, J., Koch, M. and Stolz, W. 106 W continuous-wave output power from vertical-external-cavity surface-emitting laser. English (US). *Electronics Letters* 48.9 (Apr. 2012), 516–517. ISSN: 0013-5194. DOI: 10.1049/el.2012.0531.

[26] Myara, M. Highly Coherent Single-Frequency Tunable VeCSELs: Concept, Technology, and Physical Study. *Vertical External Cavity Surface Emitting Lasers*. John Wiley & Sons, Ltd, 2021. Chap. 4, 109–143. ISBN: 9783527807956. DOI: 10.1002/9783527807956.ch4.

[27] Tropper, A. C. Recent Advances in Mode-Locked Vertical-External-Cavity Surface-Emitting Lasers. *Vertical External Cavity Surface Emitting Lasers*. John Wiley & Sons, Ltd, 2021. Chap. 8, 229–266. ISBN: 9783527807956. DOI: https://doi.org/10.1002/9783527807956.ch8.

[28] Kantola, E. Development of High-Power VECSELs for Medical Applications. PhD thesis. 2018.

[29] Kahle, H. AlGaInP-based high-performance semiconductor disk laser for the red spectral range: Gain-chip design, harmonic generation and a new laser concept. PhD thesis. 2016.

[30] Schwarzbäck, T. Epitaxie AlGaInP-baserter Halbleiterscheibenlaser: Dauerstrichbetrieb, Frequenzverdopplung und Modenkopplung. PhD thesis. 2013.

[31] Yang, Z., Albrecht, A. R., Cederberg, J. G. and Sheik-Bahae, M. Optically pumped DBR-free semiconductor disk lasers. *Opt. Express* 23.26 (Dec. 2015), 33164–33169. DOI: 10.1364/OE.23.033164.

[32] Yang, Z. Novel Concepts in Semiconductor Disk Lasers. PhD thesis. 2015. URL: http://digitalrepository.unm.edu/ose_etds/56.

[33] Phung, H.-M. Semiconductor membrane external-cavity surface-emitting lasers (MECSELs) : Power scaling, thermal management, and wavelength extension. PhD thesis. 2021. URL: https://urn.fi/URN:ISBN:978-952-03-2207-6.

[34] Fan, L., Hader, J., Schillgalies, M., Fallahi, M., Zakharian, A., Moloney, J., Bedford, R., Murray, J., Koch, S. and Stolz, W. High-power optically pumped VECSEL using a double-well resonant periodic gain structure. *IEEE Photonics Technology Letters* 17.9 (2005), 1764–1766. DOI: 10.1109/LPT.2005.853536.

[35] Moloney, J., Hader, J. and Koch, S. Quantum design of active semiconductor materials for targeted wavelengths: A predictive design tool for edge emitters and OPSLs. English (US). *Solid State Lasers XVII*. Proceedings of SPIE - The International Society for Optical Engineering. 2008. ISBN: 9780819470461. DOI: 10.1117/12.768525.

[36] Puebla, J. Spin phenomena in semiconductor quantum dots. PhD thesis. Oct. 2012.

[37] Rantaniemi, A. Design, construction and characterization of a compact vertical and lateral photoluminescence and reflection spectra measurement setup for semiconductor samples. PhD thesis. 2020. URL: https://urn.fi/URN:NBN:fi:tuni-202005225562.

[38] Hastie, J., Jeon, C., Burns, D., Hopkins, J., Calvez, S., Abram, R. and Dawson, M. A 0.5 W, 850 nm $Al_xGa_{1-x}As$ VECSEL with intra-cavity silicon carbide heatspreader. *Lasers and Electro-Optics Society, 2002. LEOS 2002. The 15th Annual Meeting of the IEEE*. Vol. 1. IEEE, 2002, 329–330. DOI: 10.1109/LEOS.2002.1134063.

[39] Cole, G. D., Nguyen, C., Follman, D., Bek, R., Zimmer, M., Witz, N., Zhang, M., Albrecht, A. R. and Sheik-Bahae, M. Chip- and Wafer-Scale Manufacturing of High-Power Membrane-External-Cavity Surface-Emitting Laser Gain Elements. *2022 Conference on Lasers and Electro-Optics (CLEO)*. 2022, 1–2.

[40] Drexler, W. and Fujimoto, J. G. Optical Coherence Tomography. Springer Cham, 2015. Chap. preface. ISBN: 978-3-319-06418-5. DOI: https://doi.org/10.1007/978-3-319-06419-2.

[41] Skinner, W. R., Hays, P. B. and Abreu, V. J. Optimization of a triple etalon interferometer. *Appl. Opt.* 26.14 (July 1987), 2817–2827. DOI: 10.1364/AO.26.002817. URL: https://opg.optica.org/ao/abstract.cfm?URI=ao-26-14-2817.

[42] *LightMachinery. Multi-Etalon Designer*. Mar. 5, 2023. URL: https://lightmachinery.com/optical-design-center/multi-etalon-designer/.

[43] Wu, Y., Sun, B. and Li, X. Semicondcutor laser active frequency stabilization technologies: a review. *Journal of the Korean Physical Society* 79 (2021), 795–809. DOI: 10.1007/s40042-021-00308-7.

[44] Kahle, H., Phung, H.-M., Tatar-Mathes, P., Rajala, P. and Guina, M. Membrane external-cavity surface-emitting lasers for high power broadband emission in the 1 µm range. *2021 27th International Semiconductor Laser Conference (ISLC)*. 2021, 1–2. DOI: 10.1109/ISLC51662.2021.9615904.

[45] Broda, A., Jeżewski, B., Sankowska and al., I. et. Growth and characterization of InP-based 1750 nm emitting membrane external-cavity surface-emitting laser. *Appl. Phys. B* 126 (2020), 192. DOI: https://doi.org/10.1007/s00340-020-07544-y.

[46] Broda, A., Jeżewski, B., Sankowska, I., Czuba, K., Kuźmicz, A. and Muszalski, J. SWIR MECSEL emitting above 1600 nm. *Vertical External Cavity Surface Emitting Lasers (VECSELs) X*. Ed. by J. E. Hastie. Vol. 11263. International Society for Optics and Photonics. SPIE, 2020, 112630I. DOI: 10.1117/12.2544883.

[47] Nürnberg, J., Alfieri, C. G. E., Waldburger, D., Golling, M. and Keller, U. Femtosecond dual-comb MIXSEL. *Vertical External Cavity Surface Emitting Lasers (VECSELs) IX*. Ed. by U. Keller. Vol. 10901. International Society for Optics and Photonics. SPIE, 2019, 109010J. DOI: 10.1117/12.2513209.

[48] Daykin, J., Woods, J. R. C., Heath, D., Bek, R., Wilkinson, J. S., Mills, B., Jetter, M., Michler, P. and Apostolopoulos, V. Membrane external-cavity surface-emitting laser emitting in bi-frequency operation through micromachining of cavity mirror. *Vertical External Cavity Surface Emitting Lasers (VECSELs) XII*. Ed. by R. G. Bedford. Vol. 12404. International Society for Optics and Photonics. SPIE, 2023, 1240403. DOI: 10.1117/12.2647363.

[49] Sheik-Bahae, M. Analysis of MECSEL mode-locking. *Vertical External Cavity Surface Emitting Lasers (VECSELs) XI*. Ed. by M. Guina. Vol. 11984. Society of Photo-Optical Instrumentation Engineers (SPIE) Conference Series. Mar. 2022, 1198405. DOI: 10.1117/12.2610991.

[50] Zhang, M., Albrecht, A. R., Truong, G.-W., Cole, G. D. and Sheik-Bahae, M. A single-mode high-power in-well pumped hybrid-MECSEL at 589 nm. *Vertical External Cavity Surface Emitting Lasers (VECSELs) XII*. Ed. by R. G. Bedford. Vol. 12404. International Society for Optics and Photonics. SPIE, 2023, 124040A. DOI: 10.1117/12.2649412.